Competition between 3D structural inheritance and kinematics during rifting: insights from analogue models

Frank Zwaan[1], Pauline Chenin[2], Duncan Erratt[2], Gianreto Manatschal[2], Guido Scheurs[1]

1) *University of Bern, Institute of Geological Sciences, Baltzerstrasse 1+3, 3012 Bern, Switzerland*
2) *Université de Strasbourg, CNRS, ENGEES, ITES UMR 7063, 5 rue Descartes, Strasbourg F-67084, France*

Email: frank.zwaan@geo.unibe.ch
Twitter: @ZwaanFrank

Keywords: Analogue modelling, multiphase rifting, continental break-up, structural inheritance

Abstract

The competition between the impact of inherited weaknesses and plate kinematics determines the location and style of deformation during rifting, yet the relative impacts of these "internal" and "external" factors remain poorly understood, especially in 3D. In this study we used brittle-viscous analogue models to assess how multiphase rifting, i.e., changes in plate divergence rate or direction, and the distribution of weaknesses in the competent mantle and crust influence rift evolution. We find that the combined reactivation of mantle and crustal weaknesses without kinematic changes creates complex rift structures. Divergence rates affects the strength of the weak lower crustal layer and hence the degree of mantle-crustal coupling. In this context slow rifting decreases coupling, so that crustal weaknesses can easily localize deformation and dominate surface structures, whereas fast rifting increases coupling so that deformation related to mantle weaknesses can have a dominant surface expression. Through a change from slow to fast rifting mantle-related deformation can overprint previous structures that formed along (differently oriented) crustal weaknesses. Conversely, a change from fast to slow rifting may shift deformation from mantle-controlled towards crust-controlled. When changing divergence directions, structures from the first rifting phase may control where subsequent deformation occurs, but only when they are well developed. Alternatively, they are ignored during subsequent rifting. We furthermore place our results in a larger framework of brittle-viscous rift modelling results from previous experimental studies, showing the importance of genral lithospheric layering, divergence rate, the type of deformation in the mantle, and finally upper crustal structural inheritance. The interaction between these parameters can lead to a large variety of deformation styles that may often lead to comparable end products. Therefore, detailed investigation of faulting and to an equal extent basin depocenter distribution over time is required to properly determine the evolution of complex rift systems. These insights provide a strong incentive to revisit various natural examples.

1. Introduction

During the early stages of continental rifting, deformation is often localized along structural weaknesses inherited from previous tectonic phases (e.g., Wilson 1966; Morley et al. 1990; Nelson et al. 1992; Bonini et al. 1997; Corti 2012). These inherited weaknesses may be situated anywhere in the lithosphere, but their impact is more significant when they are located in competent layers. Since the strength of stable thermally equilibrated continental lithosphere is generally considered be dominated by a competent upper crust and a competent upper mantle, separated by a ductile lower crustal layer (e.g., Brun 1999; Burov and Watts 2006; Burov 2011; Zwaan et al. 2019), reactivation of weaknesses in these competent layers is expected to control subsequent rift development (Chenin & Beaumont 2013).

Although tectonic modellers have often focused on the influence of either mantle or crustal weaknesses on the evolution of rift structures (e.g. Brun and Tron 1993; Le Calvez and Vendeville 2002, Bellahsen and Daniel 2005; Van Wijk 2005; Dyksterhuis et al. 2007; Autin et al. 2010, 2013; Agostini et al. 2009; Chenin and Beaumont 2013; Brune and Autin 2013; Liao and Gerya 2015; Ketterman et al. 2016; Zwaan et al. 2016, 2018a, 2019; Molnar et al. 2017, 2018, 2019; Wenker and Beaumont 2018; Chenin et al. 2019a; Duclaux et al. 2020; Meastrelli et al. 2021; Wang et al. 2021), until recently, only limited attention was directed to the question how mantle and crustal weaknesses may interact and compete during rifting, especially in three dimensions, also because 3D numerical models are relatively new. A recent analogue modelling study by Molnar et al. (2020) showed that mantle weaknesses may determine the general rift trend, whereas crustal weaknesses may segment or partition the rift structure on a smaller scale. In a subsequent publication, Zwaan et al. (2021a) improved upon this study by systematically testing how mantle and crustal weaknesses interact under constant kinematic settings. Their model results revealed the development of complex rift structures with different structural orientations under a constant kinematic setting, showing that structural weaknesses can be a highly dominant factor in a rift system. The authors pointed out, as was previously suggested by Reeve et al. (2015), that the reactivation of pre-existing crustal and mantle weaknesses during a single phase of rifting could establish a rift system with structural trends that would otherwise suggest a multiphase rifting history involving changes in large-scale plate divergence directions over time.

Yet Zwaan et al. (2021a) did not test the impact of multiphase rifting, of which previous work has shown the occurrence and importance during continental rifting (Bonini et al. 1997; Dubois et al. (2002); Henza et al. 2010, 2011; Withjack et al. (2017); Heron et al. 2019; Wang et al. 2021). Traditionally, multiphase rifting is associated with changing plate divergence directions, as has been proposed for the North Sea (Erratt et al. 1999; 2010), the Main Ethiopian Rift (Bonini et al. 1997), the Turkana Depression in East Africa (Wang et a. 2021), the Labrador Sea (Heron et al. 2019) and the Afar Rift (Chorowicz et al. 1999; Zwaan et al. 2020b, c) to refer to some examples. These changes in divergence direction are associated with a reactivation of previous rift structures, or even a clear rearrangement of structural orientations to fit the new tectonic situation. Another type of multiphase rifting involves changes in divergence rates over time. Recently, Brune et al. (2016) suggested that a systematic increase in divergence rate has occurred along various passive margins during rifting, and importantly, often > 10 Myr prior to break-up. The authors linked this increase in divergence rate to the necking of the lithosphere, which weakens the crust, allowing the assumed constant forces that drive rifting to accelerate. Yet a rift may still fail, even after attaining the necking stage (e.g., the North Sea Rift), which would imply a decrease in divergence rates as the rift system wanes. As such, we identify two endmember parameters that are generally considered to strongly affect rift evolution: (1) structural inheritance in the continental lithosphere, and (2) rifting kinematics (i.e. the rate and direction of divergence during one or more rifting phases). This amounts to comparing the impact of internal ("passive") geological parameters versus external ("dynamic") plate tectonic factors.

In order to assess the relative importance of these internal and external factors, we completed a series of brittle-viscous analogue models. In these models we first simulated the general impact of different types and orientations of structural inheritances in the crust and mantle during single-phase rift evolution; subsequently we tested the effect of changing divergence velocities as well as changing divergence directions. The model results were compared with previous work, which served to work out a general framework of the importance of various internal and external factors on rift evolution. Our main findings are that although crustal and mantle weaknesses can significantly affect rift systems, the principal factor governing rifting is the coupling between the upper crust and upper mantle, which is strongly affected by the divergence rate, as well thickness and rheology of the lower crust. By contrast, changes in divergence directions over time only have a minor impact on the morphology of rift systems if no significant pre-existing weaknesses are present. A further important observation is that various tectonic histories may lead to very similar structural arrangements, suggesting that detailed knowledge of fault activity and depocenter distribution over time is of paramount importance to reveal the true sequence of tectonic events. These insights also provide a good motivation to revisit the tectonic interpretation of a number of natural examples.

2. Methods

2.1. Materials

We applied brittle and viscous materials to simulate the continental crust (Fig. 1a, b). A 3 cm thick layer of fine quartz sand (ø 60-250 µm) was used to reproduce a 22.5 km thick brittle upper crust. The sand has an internal friction angle of 36.1˚ (Zwaan et al. 2018b), and a density of 1560 kg/m^3 when sieved from a height of ca. 30 cm (Klinkmüller et al. 2016). The sand was sieved on top of a 1 cm thick basal viscous layer consisting of a mixture of Polydimethylsiloxane (PDMS) and corundum sand, which represented a 7.5 cm thick ductile lower crust. The density of this mixture was 1600 kg/m^3 and the material had a near-Newtonian rheology, with a viscosity of 1.5·10^5 Pa·s (Zwaan et al. 2018c).

Table 1. Model materials

Granular materials	**Quartz sand**[a]	**Corundum sand**[b]
Grain size range	60-250 µm	88-125 µm
Density (specific)[c]	2650 kg/m^3	3950 kg/m^3
Density (sieved)	1560 kg/m^3	1890 kg/m^3
Angle of internal peak friction	36.1˚	37˚
Angle of dynamic-stable friction	31.4˚	32˚
Angle of reactivation friction	33.5˚	-
Cohesion	9 ± 98 Pa	39 ± 10 Pa
Viscous materials	**Pure PDMS**[a, d]	**PDMS/corundum sand mixture**[a]
Weight ratio PDMS : corundum sand	-	0.965 kg : 1.00 kg
Density	965 kg/m^3	ca. 1600 kg/m^3
Viscosity	ca. 2.8·10^4 Pa·s	ca. 1.5·10^5 Pa·s[e]
Rheology[f]	Newtonian (n = 1)	near-Newtonian (n = 1.05-1.10)

[a] Quartz sand, PDMS and viscous mixture characteristics after Zwaan et al. (2016; 2018b, c)
[b] Corundum sand characteristics after Panien et al. (2006)
[c] Specific densities after Carlo AG (2021)
[d] Pure PDMS rheology after Rudolf et al. (2016)
[e] Viscosity value holds for model strain rates < 10^{-4} s^{-1}
[f] Power-law exponent n (dimensionless) represents sensitivity to strain rate

2.2. General experimental set-up

The general set-up of our models was based on the experimental set-up previous applied by Zwaan et al. (2021a, Fig. 1). It involved a mobile base plate, attached to a mobile sidewall, the motion of which could be controlled by precise computer-guided motors. By operating these motors, the sidewall and the attached base plate could move both outward and sideward at different velocities, allowing us to implement different divergence directions and divergence rates (Fig. 1c, d). Note that the deformation we applied was asymmetric (Fig. 1, Allemand & Brun 1991).

Moving the sidewall and base plate furthermore creates a so-called velocity discontinuity (VD) along the edge of the mobile base plate. This VD has often been used to represent a weakness or fault/shear zone in the strong lithospheric mantle (e.g., Tron & Brun 1991; Brun & Tron 1993; Bonini et al., 1997; Keep and McClay, 1997; Michon and Merle, 2000; Zwaan et al. 2019; 2021a). Applying different plate geometries and thus different VD orientations allowed us to test different mantle weakness orientation with respect to the general divergence direction, as defined by angle θ_{VD} (Fig. 1c, d).

Next to these mantle weaknesses represented by the VD, we applied linear crustal weaknesses in the shape of viscous seeds (Fig. 1b, e, f) on top of the basal viscous layer. These seeds were semicircular bars (ø 5 mm) made of the same viscous material as used for the lower crustal layer. Above these seeds the brittle sand layer was locally thinner, causing a 44% weakening of the brittle layer (Zwaan et al. 2021a), leading to the localization of faulting (e.g., Le Calvez et al. 2002; Zwaan et al. 2016; 2020d; Molnar et al. 2018, 2020). Similar to the VD, we also applied different orientations for these simulated crustal weaknesses, defined as angle θ_S (Fig. 1e, f).

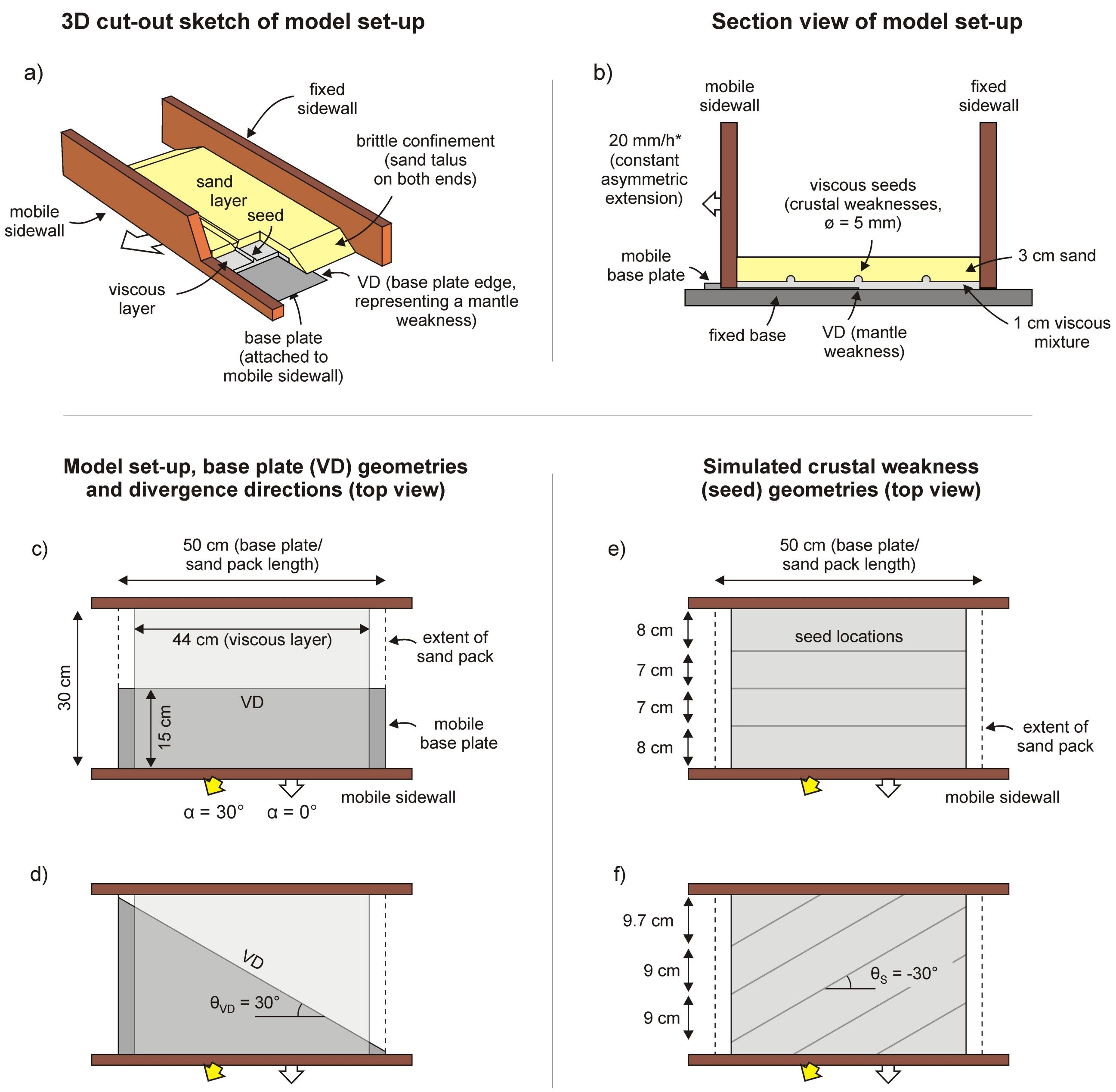

Fig. 1. ***Model set-up.*** *(a) 3D sketch of general set-up. VD: velocity discontinuity representing a weakness or fault/shear zone in the strong upper mantle. (b) Section view depicting standard model layering and the viscous seeds. (c-d) Model dimensions and base plate geometries and definition of divergence direction (defined by angle α) shown in map view. (c) Base plate configuration for series 1 (with VD parallel to model axis, or θ_{VD} = 0˚). (d) Base plate configuration for series 2 (with VD 30˚ oblique to model axis, or θ_{VD} = 30˚). (e-f) Crustal weakness geometries at the top of the viscous layer, shown in map view. (e) Model axis-parallel weaknesses (θ_S = 0˚). (f) Weaknesses -30˚ oblique to the model axis (θ_S = -30˚). * 20 mm/h is the reference divergence velocity (see Table 2). Modified after Zwaan et al. (2021a)*

2.3. Model parameters

We present a total of 30 models in five series containing six models each. The models in Series A served to establish a set of reference results for subsequent comparison with the multiphase rifting models from Series B-E (overview in Table 2). In the six reference models of Series A we tested the influence of two VD orientations (θ_{VD} = 0˚ and 30˚), as well as various seed configurations (no seeds, θ_S = 0˚ or -30˚) under constant orthogonal rifting conditions (angle α = 0˚). The divergence rate was set to be 20 mm/h over a period of 2.5 h, resulting in a total of 50 mm of divergence.

In Series B and C we tested the effects of a multiphase orthogonal rifting history (angle α = 0˚) involving changes in divergence rate. The models in these series had the same six basic initial set-ups as those in Series A, but the models were split in two phases of 25 mm of divergence each, amounting to the same 50 mm of total divergence applied in Series A. The first phase in model Series B involved slow rifting (10 mm/h), followed by a second phase of fast rifting (100 mm/h), mimicking the abrupt increase in divergence rate that occurs when a rift system starts to neck (Brune et al. 2016). Conversely, the first phase in Series C involved a fast rifting phase (100 mm/h), followed by a subsequent phase of slow rifting (10 mm/h). With this fast-to-slow divergence rate variation we aimed to simulate decreasing divergence rates in a waning rift system that failed to reach the break-up stage.

Series D and E were intended to simulate changing divergence directions over time rather than changing divergence rates, as proposed for various rift systems around the world (e.g., Bonini et al. 1997; Erratt et al. 1999, 2010). The initial model set-ups of Series D and E were the same as those used for Series A-C, but deformation was split in two phases with different directions. In Series D, initial rifting was orthogonal (α = 0˚), followed by a second phase oblique rifting (α = 30˚), whereas the models in Series E follow the inverse sequence: initial oblique rifting followed by orthogonal rifting. In both series, the divergence rate was kept the same as in the reference models (20 mm/h). Each phase involved 25 mm of stretching in the direction of divergence, for a total of 50 mm of divergence (so that overall stretching in the model is ca. 17%, i.e., β = ca. 1.2).

Note that several of the 30 model set-ups presented in this work were run multiple times with very similar results indicating good reproducibility. A complete dataset including all extra models can be found in the supplementary material (Zwaan et al. 2021b).

Table 2. Overview of model parameters

Model series	Model name	Weakness orientation		Direction and rate of divergence			
		VD (angle θ_{VD})	Seeds (angle θ_S)	Phase 1 (First 25 mm of divergence)*		Phase 2 (Second 25 mm of divergence)*	
				Direction (angle α)	Rate (v) in mm/h	Direction (angle α)	Rate (v) in mm/h
Series A*	A1	0°	-	0°	20	0°	20
Reference models with constant parameters	A2	0°	0°	0°	20	0°	20
	A3	0°	-30°	0°	20	0°	20
	A4	30°	-	0°	20	0°	20
	A5	30°	0°	0°	20	0°	20
	A6	30°	-30°	0°	20	0°	20
Series B	B1	0°	-	0°	100	0°	10
Slow-to-fast rifting models	B2	0°	0°	0°	100	0°	10
	B3	0°	-30°	0°	100	0°	10
	B4	30°	-	0°	100	0°	10
	B5	30°	0°	0°	100	0°	10
	B6	30°	-30°	0°	100	0°	10
Series C	C1	0°	-	0°	100	0°	10
Fast-to-slow rifting models	C2	0°	0°	0°	100	0°	10
	C3	0°	-30°	0°	100	0°	10
	C4	30°	-	0°	100	0°	10
	C5	30°	0°	0°	100	0°	10
	C6	30°	-30°	0°	100	0°	10
Series D	D1	0°	-	0°	20	30°	20
Orthogonal-to-oblique rifting models	D2	0°	0°	0°	20	30°	20
	D3	0°	-30°	0°	20	30°	20
	D4	30°	-	0°	20	30°	20
	D5	30°	0°	0°	20	30°	20
	D6	30°	-30°	0°	20	30°	20
Series E	E1	0°	-	30°	20	0°	20
Oblique-to-orthogonal rifting models	E2	0°	0°	30°	20	0°	20
	E3	0°	-30°	30°	20	0°	20
	E4	30°	-	30°	20	0°	20
	E5	30°	0°	30°	20	0°	20
	E6	30°	-30°	30°	20	0°	20

* Series A models were run continuously for 50 mm total divergence without change in parameters, hence in these models, phase 2 was simply a direct continuation of phase 1

2.4. Analysis techniques

The surface evolution of all models was monitored by means of time-lapse photography. A Nikon D200 (10 MP) camera provided map view images, and two obliquely oriented Nikon D810 (36.3 MP) cameras on both sides of the centrally mounted Nikon D200 allowed for a stereoscopic view of the model. These cameras were all linked to a central computer and simultaneous remote-controlled pictures were taken every minute (after every 1/3 mm of divergence for the 20 mm/h rifting models, and after each 1/6 mm of divergence for the 10 mm/h rifting models), except for the models with a divergence rate of 100 mm/h, which were photographed every 1.5 min (hence after each 5 mm of divergence) due to practical limitations. We applied a 4 x 4 cm grid of thin < 1 mm thick corundum sand on the model surface for visual assessment of horizontal displacements.

Next to providing a general visual impression of surface model evolution, these photographs also allowed a more detailed analysis and quantification of model surface deformation through means of Particle Image Velocimetry (PIV) techniques (e.g. Adam et al., 2005, Boutelier et al. 2019, and references therein). This PIV analysis was done through a comparison of the high-resolution Nikon D810 time-lapse pictures in LaVision DaVis 10.2 PIV software (after correcting for image warping due to the obliquity of the images by systematically adopting the back-warping procedure applied to a reference plate of known dimensions). This software allowed us to extract horizontal displacements over time. These horizontal displacement data were subsequently used to create incremental maximum normal strain maps (increments of 5 mm of deformation), which we took as a proxy to trace active deformation in the model over time.

In addition to the PIV-based strain analysis, we used the pairs of synchronous oblique high-quality Nikon D810 time-lapse photographs to reconstruct model topography in high detail. Fixed markers with known coordinates were used to geo-reference the pictures in Agisoft PhotoScan photogrammetry software, yielding digital elevation models (DEMs). These DEMs allowed the visualization of topographic changes, notably rift basin generation over time, which could be directly compared to the PIV results for a more complete understanding of model evolution.

2.5. Scaling

Standard model scaling procedures serve to ensure that laboratory experiments adequately represent the natural prototype. Since the rheology of brittle materials is strain rate-independent, the angle of internal friction of our sand was the main concern for scaling purposes. This angle (36.1˚) is very similar to values found in upper crustal rocks (31-38˚, Byerlee 1978, Table 3). Scaling viscous materials is more complex than brittle materials since their strain rate-dependent rheology needs to be taken into account. With the stress ratio between model and nature (σ^*, convention: $\sigma^* = \sigma_{model}/ \sigma_{nature}$): $\sigma^* = \rho^* \cdot h^* \cdot g^*$, where ρ^*, h^* and g^* are density, length and gravity ratios, respectively (Hubbert 1937; Ramberg 1981) and the viscosity ratio (η^*) we can acquire the strain rate ratio $\dot{\varepsilon}^*$ (Weijermars & Schmeling 1986): $\dot{\varepsilon}^* = \sigma^*/\eta^*$. The strain rate ratio subsequently allows us to derive the velocity and time ratios (v^* and t^*): $\dot{\varepsilon}^* = v^*/h^* = 1/t^*$. Adopting a relatively high lower crustal viscosity of ca. $5 \cdot 10^{21}$ Pa.s that may be typical for early magma-poor rift systems, e.g., Buck 1991), one hour in our models scales up to ca. 3 Myr in nature, and our reference divergence rate of 20 mm/h translates to ca. 5 mm/yr. Our slow divergence rates (10 mm/h) then translate to ca. 2.5 mm/y, and fast rifting (100 mm/h) to ca. 25 mm/yr. These slow divergence rates are very similar to typical rift divergence rates in continental rifts (e.g., Saria et al. 2014), whereas the scaled fast divergence rates are in accordance with the accelerated divergence rates reported by Brune et al. (2016). An overview of scaling parameters is provided in Table 3.

In addition, we examine the dynamic similarity of the model and the natural example. We can derive the dynamic similarity between the brittle model layer and its upper crustal equivalent using the ratio Rs between the gravitational stress and the cohesive strength or cohesion C (Ramberg 1981; Mulugeta 1998): R_s = gravitational stress/cohesive strength = $(\rho \cdot g \cdot h)/C$. Assuming a natural cohesion of 12 MPa for upper crustal rocks, together with a 9 Pa cohesion in the sand, we find a R_s of 51 for both model and nature. Although this naturel cohesion value of 12 MPa is slightly lower than cohesions obtained from rock deformation tests (e.g., Handin, 1969; Jaeger & Cook 1976; Twiss & Moore 1992), we consider it quite acceptable since the strength of the lithosphere has generally decreased during preceding deformation phases. The Ramberg number R_m applies for dynamic similarity scaling of viscous materials (Weijermars & Schmeling 1986): R_m = gravitational stress/viscous strength = $(\rho \cdot g \cdot h^2)/(\eta \cdot v)$, and we find a value of 17 for both the viscous mixture and its lower crustal equivalent in nature. Since both the R_s and R_m values of our models are practically the same as in their natural equivalent, we consider our models properly scaled for simulating continental rifting.

Table 3. Scaling parameters

		Model	**Nature**
General parameters	Gravitational acceleration (g)	9.81 m/s^2	9.81 m/s^2
	Divergence velocity (v)	$5.6 \cdot 10^{-5}$ m/s*	$1.6 \cdot 10^{-10}$ m/s
Brittle layer	Material	Quartz sand	Upper crust
	Peak internal friction angle (φ)	36.1°	30-38°
	Thickness (h)	$3 \cdot 10^{-2}$ m	$2.25 \cdot 10^{4}$ m
	Density (ρ)	1560 kg/m^3	2800 kg/m^3
	Cohesion (C)	9 Pa	10^{7} Pa
Viscous/ ductile layer	Material	PDMS/corundum sand mixture	Lower crust
	Thickness (h)	$1 \cdot 10^{-2}$ m	$7.5 \cdot 10^{4}$ m
	Density (ρ)	1600 kg/m^3	2900 kg/m^3
	Viscosity (η)	$1.5 \cdot 10^{5}$ Pa·s	$5 \cdot 10^{21}$ Pa·s
Dynamic scaling values	Brittle stress ratio (R_s)	51	51
	Ramberg number (R_m)	17	17

* Divergence velocity in the reference models (Series A, v = 20 mm/h, see Table 2)

3. Results

We present the results of our model analysis in a series of overview figures (Figs. 2-6). These figures show the incremental maximum normal strain as derived from PIV analysis over an divergence increment of 5 mm at the start and end of each deformation phase. The model surface topography at the end of each deformation phase is included as well. We first discuss the reference models from Series A, and then the multiphase rifting models from Series B-E.

3.1. Series A – Reference models

The results from our Series A models with a constant divergence direction (α = 0˚) and a constant divergence rate of 20 mm/h provide a reference framework for the subsequent analysis of multiphase rifting models (Fig. 2).

3.1.1. Model axis-parallel VD Models A1-3

Model A1, involving an axis-parallel VD set-up (θ_{VD} = 0˚) without seeds, developed two deformation zones on both sides of the VD during the initial stages of the experimental run (Fig. $2a_{I}$). Subsequently, strain localized along normal faults and a narrow double graben system developed (Fig. $2a_{II,\ III}$). As stretching continued, the rift structure grew wider due to the start of new faulting on the moving base plate, leading to the formation of an additional graben, whereas fault activity on the opposite side of the graben diminished notably (Fig. $2a_{IV\text{-}VI}$). Some boundary effects are visible on both sides of the model.

Adding model-axis parallel seeds (θ_{S} = 0˚) in Model A2 considerably affected the central graben structure as seen in Model A1 by diverting deformation away from the VD (Fig. 2a, b). Initial deformation strongly localized along the outermost seeds, forming through-going grabens, in contrast to the various grabens developing in the central part of the model (Fig. $2b_{I\text{-}III}$). This structural arrangement was established early on and remained in place during subsequent stretching (Fig. $2b_{IV\text{-}VI}$), but no clear migration of deformation onto the moving base plate as in Model A1 was observed (Fig. 2a, b). Some boundary effects are visible on both sides of the model.

Applying oblique seeds (θ_{S} = -30˚) in model A3, rather than model-axis parallel seeds, also disrupts the central rift structure from Model A1, but in a different fashion than in Model A2 (Fig. 2a-c). Whereas the early stages of Model A3 developed similar deformation bands on both sides of the VD as in Model A1 (Fig. $3a_{I}$, $2b_{I}$), the oblique seeds localized deformation early on, leading to the establishment of a series of oblique grabens (Fig. $3c_{I\text{-}III}$). Meanwhile, the deformation zones from the earlier stage developed into a series of grabens that were interrupted and segmented by the seed-induced graben structures (Fig. $3c_{I\text{-}III}$). Like in Model A2, this structural arrangement was formed early on and remained stable during the following 25 mm of stretching, although we did observe a slight migration of strain onto the moving base plate over time, and the formation of more pronounced boundary effects (grabens) along the lower sidewall (Fig. $3c_{IV\text{-}VI}$).

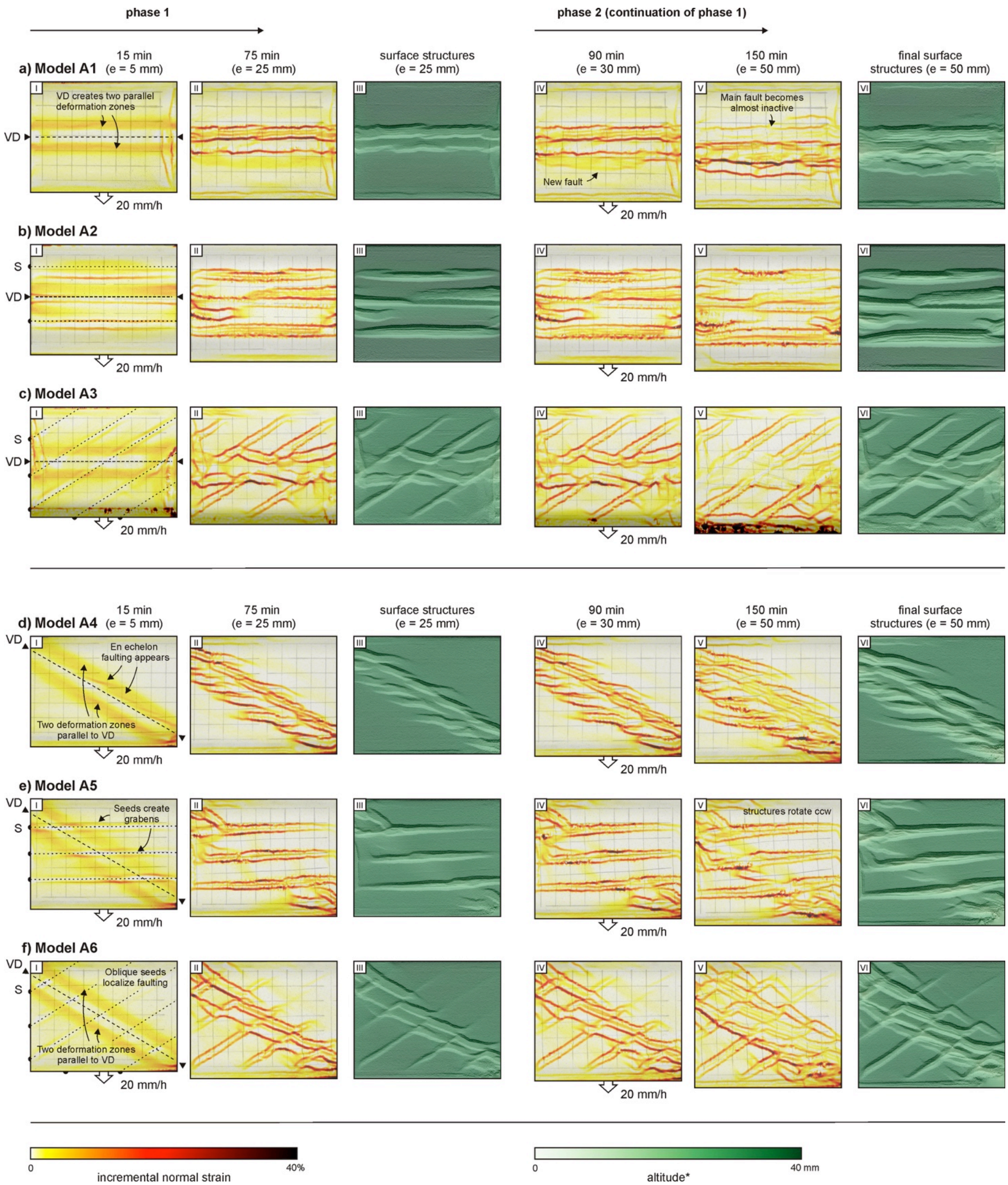

Fig. 2. *Model PIV and topography analysis results from reference Series A with a constant orthogonal rifting (α = 0˚) and a constant divergence rate of 20 mm/h˚). Divergence increments for PIV analysis were 5 mm. VD: velocity discontinuity, S: seeds.*

3.1.2. Oblique VD Models A4-6

The use of an oblique VD in Model A4 (θ_{VD} = 30˚, without seeds) led to the development of a very different structure than that observed in its equivalent with a model axis-parallel Model A1 (Fig. 2a, d). Although Model A4 does form initial deformation zones along the VD (similar to those in Model A1, Fig. $2a_{I}$, d_{I}), these develop into two series of en echelon grabens on both sides of the oblique VD, instead of a through-going rift structure with long normal faults from Model A1 (Fig. 2a, d). As deformation continued, the oblique rift structure grew significantly wider, and a slight shift of strain onto the moving base plate was observed (Fig. $2d_{IV\text{-}VI}$).

Similar to Models A2 and A3, the introduction of seeds in models with an oblique VD strongly affected the evolution of our rift structures (Fig. 2b, c, e, f). Model A5 shows how the presence of rift axis-parallel seeds (θ_{S} = 0˚) almost completely overprints the VD-induced structures: whereas the initial double deformation zones form early on, the seeds also localize deformation early on (Fig. $2e_{I}$) and attract most of the subsequent deformation in Model A5 (Fig. $2e_{II\text{-}VI}$). In contrast to Model A5, the VD still has an important control in Model A6 (Fig. 2f) since the presence of -30˚ oblique seeds did not prevent the development of the dual VD-parallel deformation zone (Fig. $2e_{I}$, $2f_{I}$). Yet their early activation did, in a similar fashion to model A3, segment and interrupt the rift structure along the VD from an early stage on (Fig. $2f_{II,\ III}$). During subsequent deformation, a complex distribution of oblique grabens developed, with an apparent migration of deformation onto the moving base plate (Fig. $2f_{IV\text{-}VI}$).

3.2. Series B – Slow-to-fast rifting models

Here we present the results from our series B models involving an initial phase of slow rifting (10 mm/h), followed by a second phase of fast rifting (100 mm/h) (Fig 3). The divergence direction throughout the model runs was kept constant (angle α = 0˚).

3.2.1. Model axis-parallel VD Models B1-3

The results from Model B1 show how initial slow divergence rates affect an experiment with a model-parallel VD (θ_{VD} = 0˚) and no seeds (Fig. $3a_{I\text{-}III}$). The model developed similar deformation zones as those in reference Model A1 (Fig. $2a_{I}$), but these had a wider spacing in Model B1 (Fig. $3a_{I}$). As a result, the rift structure in Model B1 was wider, consisting of two separated grabens instead of a central rift zone (Fig. $2a_{I}$, $3a_{I}$). During the subsequent phase of fast rifting, the style of deformation changed considerably (Fig. $3a_{IV\text{-}VI}$). Faulting was much more concentrated along the VD, leading to the overprinting of the initial wide rift structure by a narrow rift basin.

The divergence rate had a clear influence on how well seeds localize deformation. During the initial slow rifting phase in Model B2, the rift axis-parallel seeds (θ_{S} = 0˚) localized rifting better than in reference Model A2, forming a series of spaced-out grabens (Fig. $2b_{I\text{-}III}$, $3b_{I\text{-}III}$). And similar to Model B1, the subsequent fast rifting phase overprinted this wide rift structure with a narrow rift basin (Figs. $3a_{IV\text{-}VI}$, $3b_{IV\text{-}VI}$). The same tendencies were observed in Model B3 with -30˚ oblique seeds: initially the seeds localized deformation very well, even though somewhat en echelon VD-parallel rift zones formed, which evolved into offset grabens similar to those observed in reference Model A3 (Fig. $3c_{I\text{-}III}$, $3c_{I\text{-}III}$). But subsequent fast rifting caused an overprinting effect by the VD, creating a clearly defined central rift basin (Fig. $3c_{IV\text{-}VI}$).

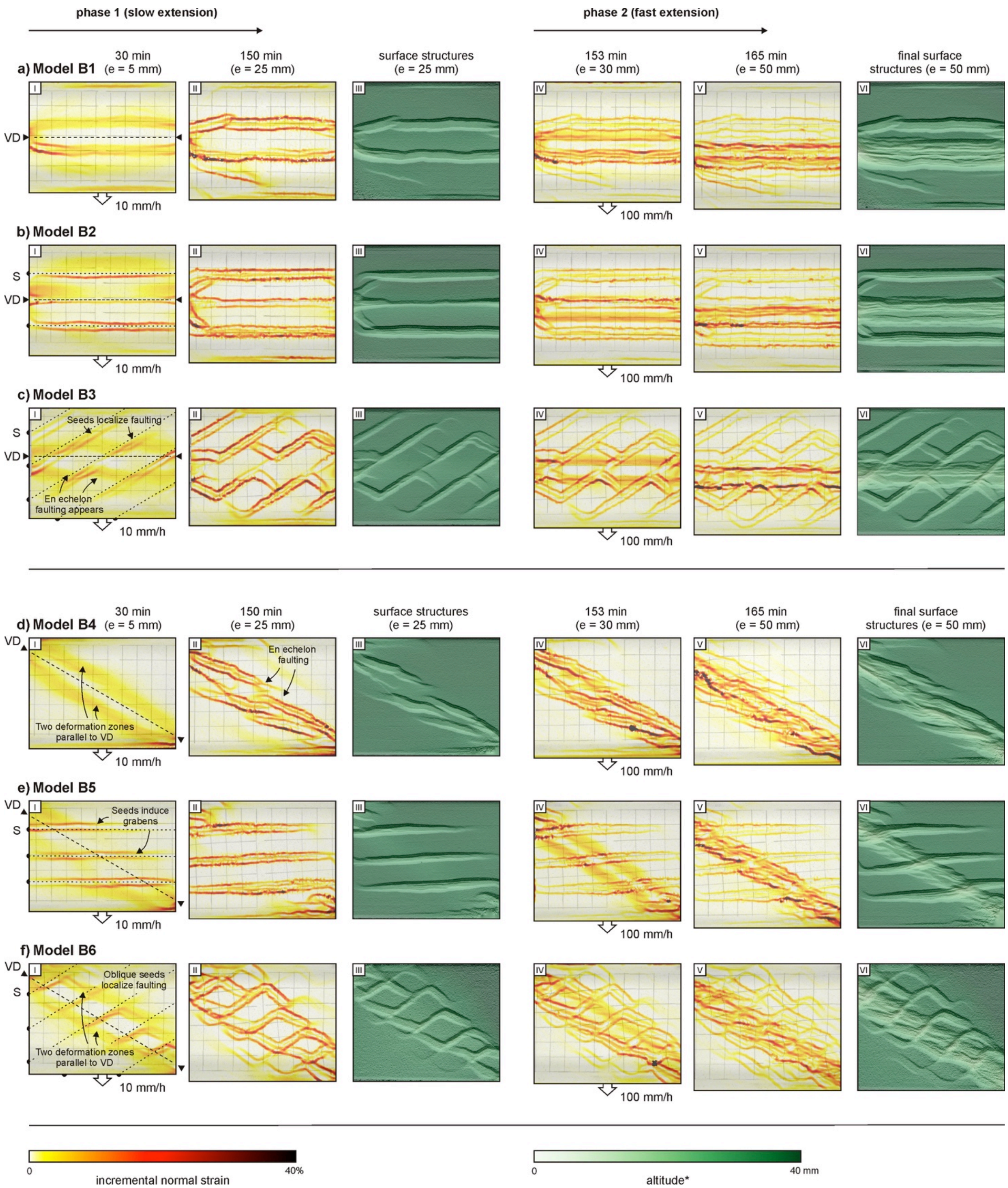

__Fig. 3.__ Model PIV and topography analysis results from Series B involving a first phase of slow rifting (10 mm/h) followed by a second phase of fast rifting (100 mm/h). The divergence direction was orthogonal during both phases (α = 0˚). ˚). Divergence increments for PIV analysis were 5 mm. VD: velocity discontinuity, S: seeds.

3.2.2. Oblique VD Models B4-6

The presence of a 30˚ oblique VD in absence of seeds resulted in the development of initial VD-parallel diffuse deformation zones that later on localized en echelon faulting during the first slow rifting phase in Model B4 (Fig. $3d_{I-III}$). The occurrence of these deformation zones was similar to those observed in reference Model A4, yet the en echelon arrangement was much less intricate in Model B4 (Fig. $4d_{I-III}$). When applying fast divergence during the second phase, strain became mostly concentrated along the VD (Fig. $4d_{IV-VI}$).

As previously observed in Models A5 and A6, seeds tend to strongly localize deformation when initial divergence rates are slow (Figs. $3e_{I-III}$, $3f_{I-III}$). In Model B5, we found that the model axis-parallel seeds (θ_S = 0˚) were even more dominant than in Model A5, up to the point that the influence of the VD was negligible (Figs. $2e_{I-III}$, $3e_{I-III}$). In Model B6 the -30˚ oblique seed-induced grabens had much greater influence on the rift structure than in Model A6, even though the VD in model B6 did localize initial deformation zones and caused the general structure to follow a 30˚ oblique path (Figs. $2f_{I-III}$, $3f_{I-III}$). Yet similar to Models A5 and A6 (Figs. $2e_{IV-VI}$, $3e_{IV-VI}$), the subsequent fast divergence in Models B5 and B6 strongly concentrated deformation, overprinting the structures formed during the initial slow phase with a highly localized rift basin along the VD (Figs. $2e_{I-III}$, $3e_{I-III}$).

3.3. Series C – Fast-to-slow rifting models

In this section we describe the results from our series C models with an initial phase of fast rifting (100 mm/h), and a subsequent phase of slow rifting (10 mm/h) (Fig 4). The divergence direction was constant during the experimental runs (angle α = 0˚).

3.3.1. Model axis-parallel VD Models C1-3

The results from the second, fast rifting phase model in Series B suggest that fast rifting localizes deformation along the VD (Fig. 3), and we found a similar effect in our Model C1 with a model-axis parallel VD and no seeds (Fig. 4a). During the initial rift phase, the two deformation bands previously observed in reference model A1 developed (Figs. $2a_I$, $4a_I$), but the subsequent (double) rift structure was clearly narrower (Figs. $2a_{II-III}$, $4a_{II-III}$). In the following slow rifting phase, strain was however very much distributed, and the final rift structure was much wider than the initial narrow basin (Fig. $4a_{II-III}$).

The same concentration of deformation during initial fast rifting is observed in Models C2 and C3 (Fig. $4b_{I-III}$, $4c_{I-III}$). In these models, most deformation is concentrated in the initial deformation bands along the VD that subsequently develop into a narrow rift basin, whereas the seeds attracted only very limited deformation (Fig. $4b_{I-III}$, $4c_{I-III}$). Yet as soon as the divergence rate dropped during the second phase, deformation became primarily concentrated along the seeds (Fig. $4b_{IV-VI}$, $4c_{IV-VI}$). Note how the final structures in these models are very similar to these from Series B (Figs. 3, 4).

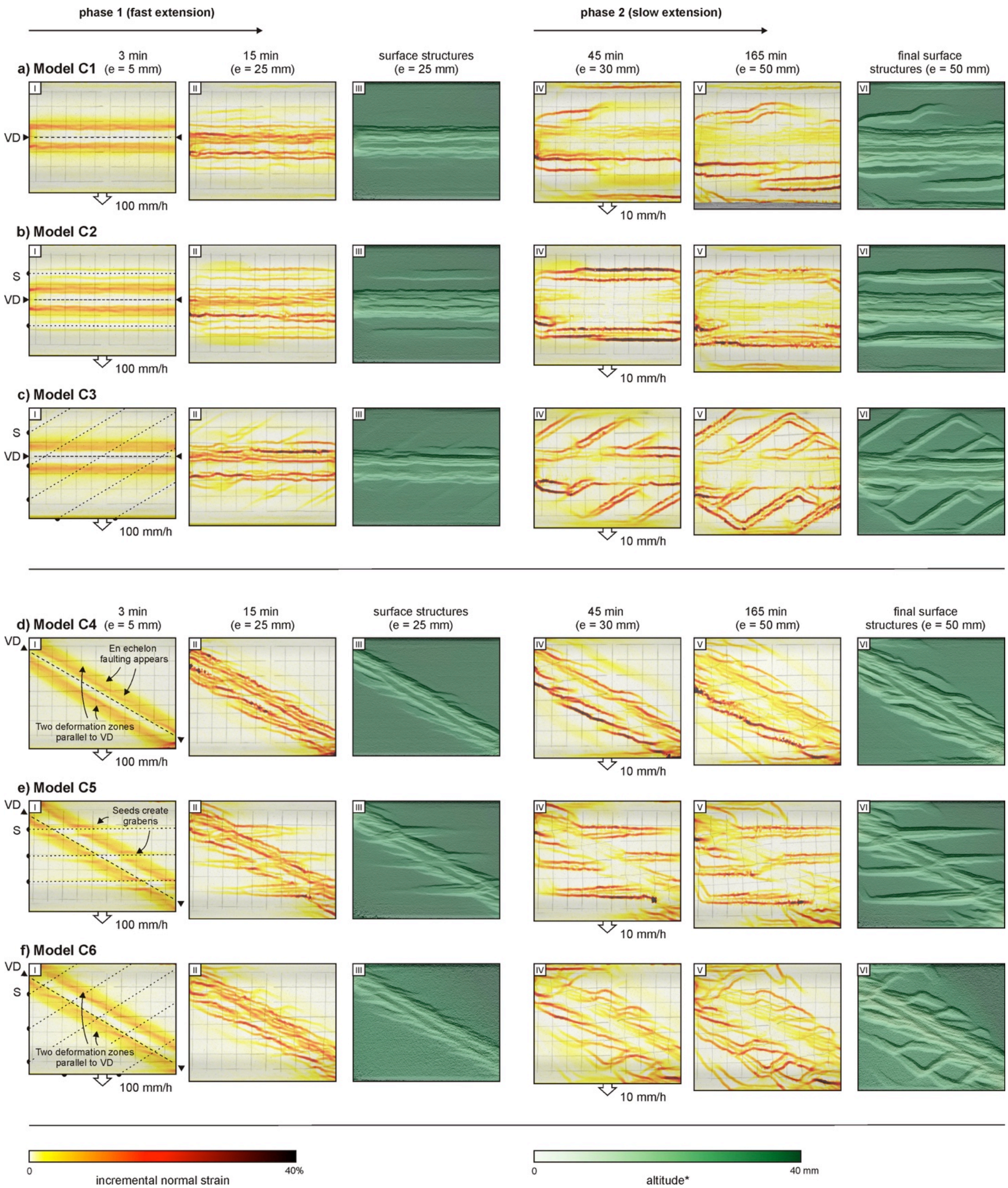

Fig. 4. *Model PIV and topography analysis results from Series C involving a first phase of fast rifting (100 mm/h) followed by a second phase of slow rifting (10 mm/h). The divergence direction was orthogonal during both phases (α = 0˚). Divergence increments for PIV analysis were 5 mm. VD: velocity discontinuity, S: seeds.*

3.3.2. Oblique VD Models C4-6

Models C4-6 with a 30˚ oblique VD showed very similar reactions to divergence rate as described in the previous section (Fig. 4). Model C4, without seeds, formed deformation zones along the VD during the initial fast rifting phase, which resulted in a rift basin along the VD that was more concentrated than its counterpart in reference Model A4 as it largely lacked the en echelon arrangement of the latter (Figs. $2d_{I\text{-}III}$, $4d_{I\text{-}III}$). Yet when exposed to slow rifting, deformation became much more distributed, as previously observed in Model C1 (Fig. $4a_{IV\text{-}VI}$, $4d_{IV\text{-}VI}$).

The seeds in Models C5 and C6 have similar reactions to the changes in divergence rate observed in Models C2 and C3 (Fig. 4b, c, e, f); During the initial fast rifting phase, deformation is strongly concentrated along the initial deformation zones and subsequent faults along VD, whereas the seeds show barely any strain localization (Fig. $4e_{I\text{-}III}$, $4f_{I\text{-}III}$). This is in stark contrast to the dominance of the seeds in the equivalent reference models and models with initial slow rifting (Figs. 2e, f, 3e, f). Yet similar to models C2 and C3, when the strain rate was decreased in the second phase, Models C5 and C6 showed a significant shift towards broader, more distributed deformation and localization of deformation along the seeds. Seed-related structures became more pronounced in Model C5 than in Model C6 (Fig. 4b, c, d, e). It is furthermore worth noting that also the final structures in these models are very similar to these from Series B (final topography in Fig. 3, 4).

3.4. Series D – Orthogonal-to-oblique rifting models

Our Series D models included an initial phase orthogonal rifting (α = 0˚), followed by a phase of oblique rifting (α = 30˚) (Fig 5). The divergence rate was the same as in the reference models (20 mm/h).

3.4.1. Model axis-parallel VD Models D1-3

The boundary conditions in the early stages of Models D1-3 with a model axis-parallel VD (Fig. 5a-c) were the same as in reference Models A1-3 (Fig. 2a-c), and therefore the results were fairly similar. There are some minor differences in timing of fault initiation (compare Model A1 with Model D1) and the structures are not exactly the same (notably the extra graben in Model D1). Yet the models provide a good match, which highlights the consistency of our model approach. As these models continued to develop during a second phase of 30˚ oblique rifting the overall graben arrangement did not deviate much from the arrangement established during the first phase, (Fig. 2a-c), and as such the overall results from Models D1-3 are in general very similar to the structures observed in the reference models A1-3 (Figs. 2a-c, 5a-c).

3.4.2. Oblique VD Models D4-6

Similar to Models D1-3, the initial orthogonal rifting phase in Models D4-6 with a 30˚ oblique VD yielded very similar results to reference models A4-6 (Figs. 2d-f, 5d-f). These models did largely reuse the structures established from the first phase during the second, 30˚ oblique rifting phase. A small exception to the rule is the development of two grabens oriented sub-parallel to the VD in Model D4 (Fig. $5e_{IV\text{-}VI}$).

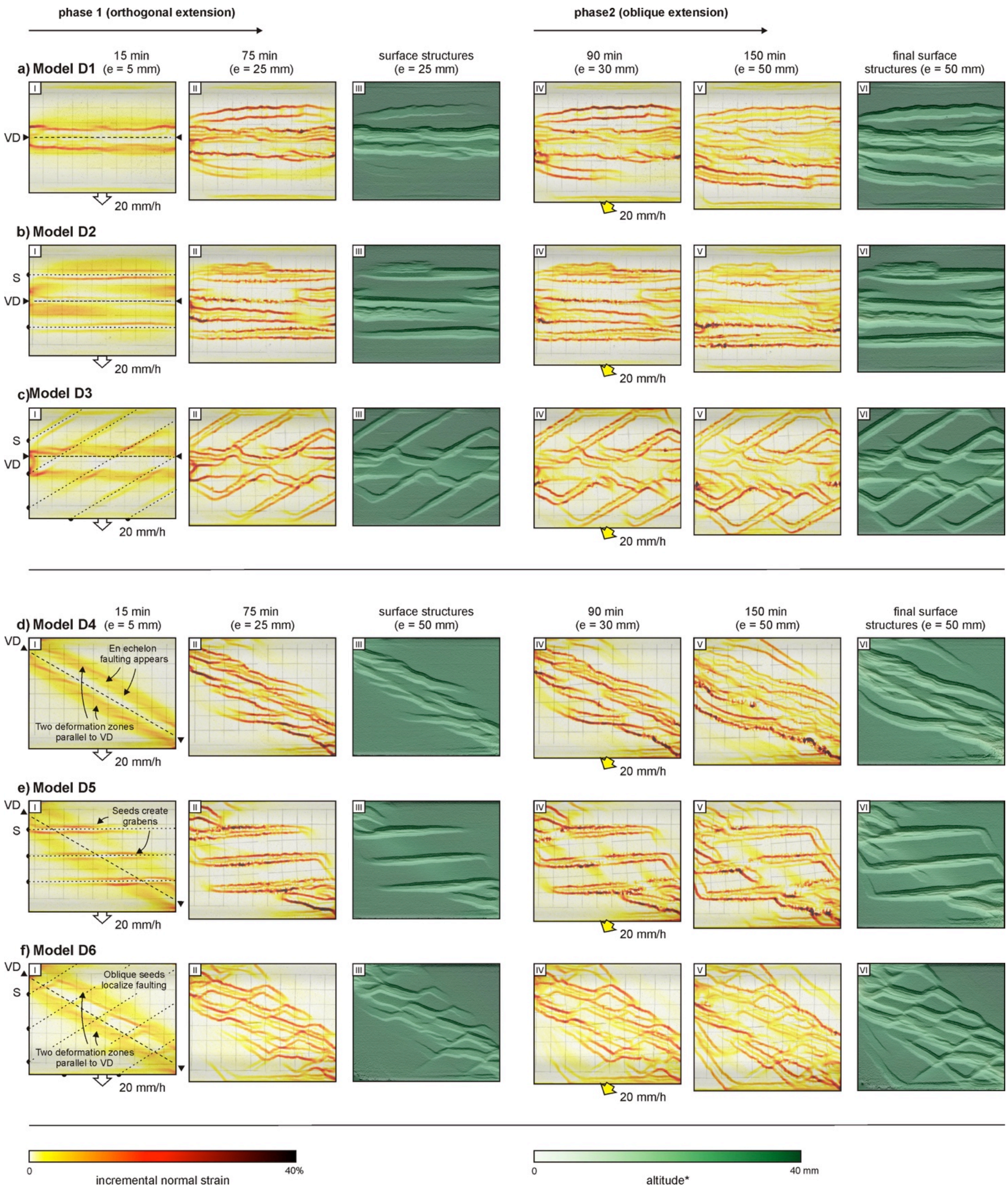

Fig. 5. *Model PIV and topography analysis results from Series C involving a first phase of orthogonal rifting (α = 0˚) followed by a second phase of oblique rifting (α = 30˚). The divergence rate was constant (20 mm/h) during both phases˚). Divergence increments for PIV analysis were 5 mm. VD: velocity discontinuity, S: seeds.*

3.5. Series E – Oblique-to-orthogonal rifting models.

The final results are from Series E, which includes models with initial 30˚ oblique rifting, followed by an orthogonal rifting phase (α = 0˚) (Fig 6), with the divergence rate being kept the same at 20 mm/h.

3.5.1. Model axis-parallel VD Models E1-3

Initial oblique rifting had a clear effect on Model E1 with a model axis-parallel VD but without seeds, when compared to its reference equivalent, Model A1 (Figs. 2a, 6a). In this model, the early deformation zones developed, with en echelon grabens forming towards the end of the first phase (Fig. $6a_{I-III}$). After a shift to orthogonal rifting, the en echelon grabens continued to be active, but new faults and grabens showed a tendency to grow sub-perpendicular to the new divergence direction (Fig. $6a_{IV-VI}$).

Yet when seeds were present in Models E2 and E3 (Fig. 6b, c), these strongly controlled where deformation was localized, resulting in structures that were very similar to the reference Models A2 and A3 (2b, c). There is however some variation in Model E3, in the shape of more grabens between the seed-induced structures, opening sub-perpendicular to the divergence direction.

3.5.2. Oblique VD Models E4-6

Oblique rifting Model E4 with a 30˚ oblique VD had an initial divergence direction perpendicular to the VD (Fig. $6d_{I-III}$). As a result, the VD-parallel strain zones developed two grabens on both sides of the VD (Fig. $6d_{I-III}$), rather than the en echelon graben arrangement in reference model A4 (Fig. $2d_{I-III}$). The first phase in Model E4 also generated some faint strain zones farther away from the central VD-aligned grabens (Fig. $6d_{II}$). These latter strain zones subsequently develop into secondary graben during the second orthogonal rifting phase, without clear indications of a change of deformation style (Fig. $6d_{IV-VI}$).

In Models E5 and E6, seed activation is affected by initial oblique rifting (Fig. $6e_{I-III}$, f_{I-III}). In comparison to reference Models A5 and A6 (Fig. $6e_{I-III}$, f_{I-III}), the seeds in these Series 5 models are poorly reactivated whereas the VD-induced grabens are significantly better developed. During the second phase of orthogonal rifting, the seeds become dominant in Model E5, and deformation becomes rather distributed in model E6. The final structures in Models E5 and E6 are overall very similar to those in reference models A5 and A6 (Figs. $2e_{VI}$, f_{VI}, $6e_{VI}$, $6f_{VI}$).

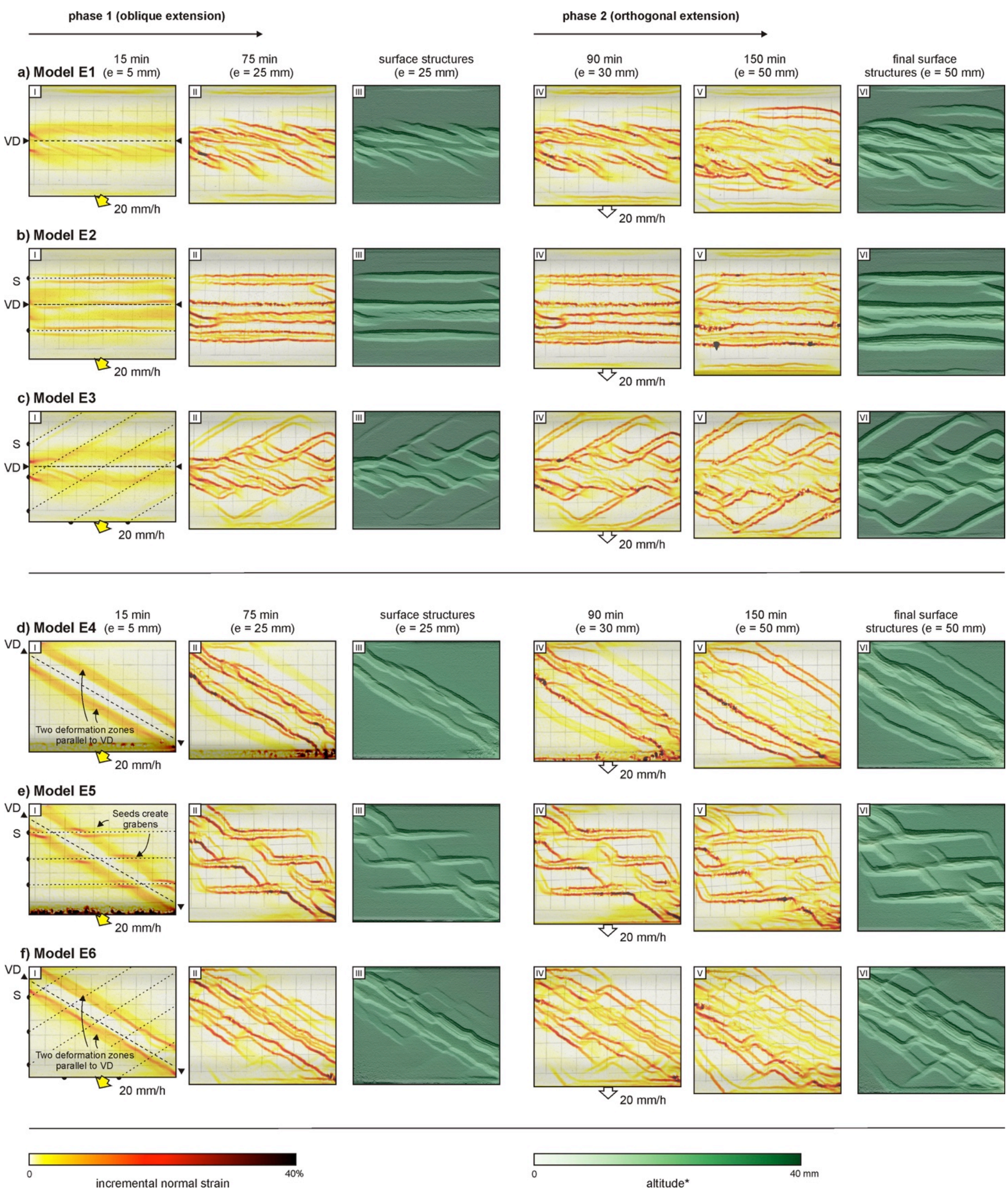

Fig. 6. *Model PIV and topography analysis results from Series C involving a first phase of oblique rifting (α = 30˚) followed by a second phase of orthogonal rifting (α = 0˚). The divergence rate was constant (20 mm/h) during both phases˚). Divergence increments for PIV analysis were 5 mm. VD: velocity discontinuity, S: seeds.*

4. Discussion

4.1. Synopsis of model results

We present an overview of our model results in Figs. 7 and 8, which form a basis for the synopsis outlined in the following sections. The first figure is a compilation of maximum normal strain data whereas the latter figure summarizes topography analysis results. These overview figures include data from all reference models, but for the multiphase rifting models, we focus on the results from experiments with a model-axis parallel VD (θ_{VD} = 0˚), the results of which, despite some minor details, are representative for the oblique VD models as well. A full overview of all model results (regarding both strain and topography) is provided in the Appendix (Figs. A1 and A2).

4.1.1. Reference models

The results of the reference models from model Series A provide clear insights into the influence of VD and seed geometry on rift structures (Figs. 7a-f, 8a-f). We found that without seeds, a model axis-parallel VD (θ_{VD} = 0˚) tends to form a central (double) rift structure with through-going faults, in contrast to the en echelon graben structures developing along an oblique VD (Figs. 7a, d, 8a, d). These results are clearly related to the divergence direction with respect to the VD (orthogonal vs. oblique). Yet adding seeds diverted deformation away from the VD-induced grabens (Figs. 7b, c, e, f, 8b, c, e, f). A clear competition between the VD and seeds occurred, highlighting that the structural trends related to weaknesses oriented orthogonally to the divergence direction dominated the model surface expression in our experiments (e.g., compare Model A2 to Model A5, in Fig. 7 and 8). The seeds furthermore induce segmentation of the VD-related rift zone and create a rift arrangement with different structural orientations.

4.1.2. Effects of divergence rate variations

The models from Series B and C provide clear insights into the effects of changing divergence rates during rifting (Figs. 7g-l, 8g-l). With respect to the reference models with intermediate divergence rates (Figs. 7a-e, 8a-e), slow (10 mm/h) rifting resulted in (widely) distributed deformation, and in models with seeds, slow rifting caused increased activation of faulting along these seeds compared to models with higher extension rates. By contrast, models involving fast rifting (100 mm/h) revealed very strong localization of deformation along the VD. This relation between divergence rate and the development of structures along either the VD or seeds is especially well illustrated by the strain maps (Fig. 7g-l). Strikingly, the order of the divergence rate variations did not cause significant differences in this relation: both deformation regimes simply overprinted the previously established structures (Figs. 7g-l, 8g-l). As a result, the final structures in the models with changing divergence rates but with the same general set-up were very similar, even if their evolution was very different (e.g., compare Model B2 to Model B6, Fig. 8h, k). In fact, the final structures were also very similar to those found in the reference models (Fig. 8a-f).

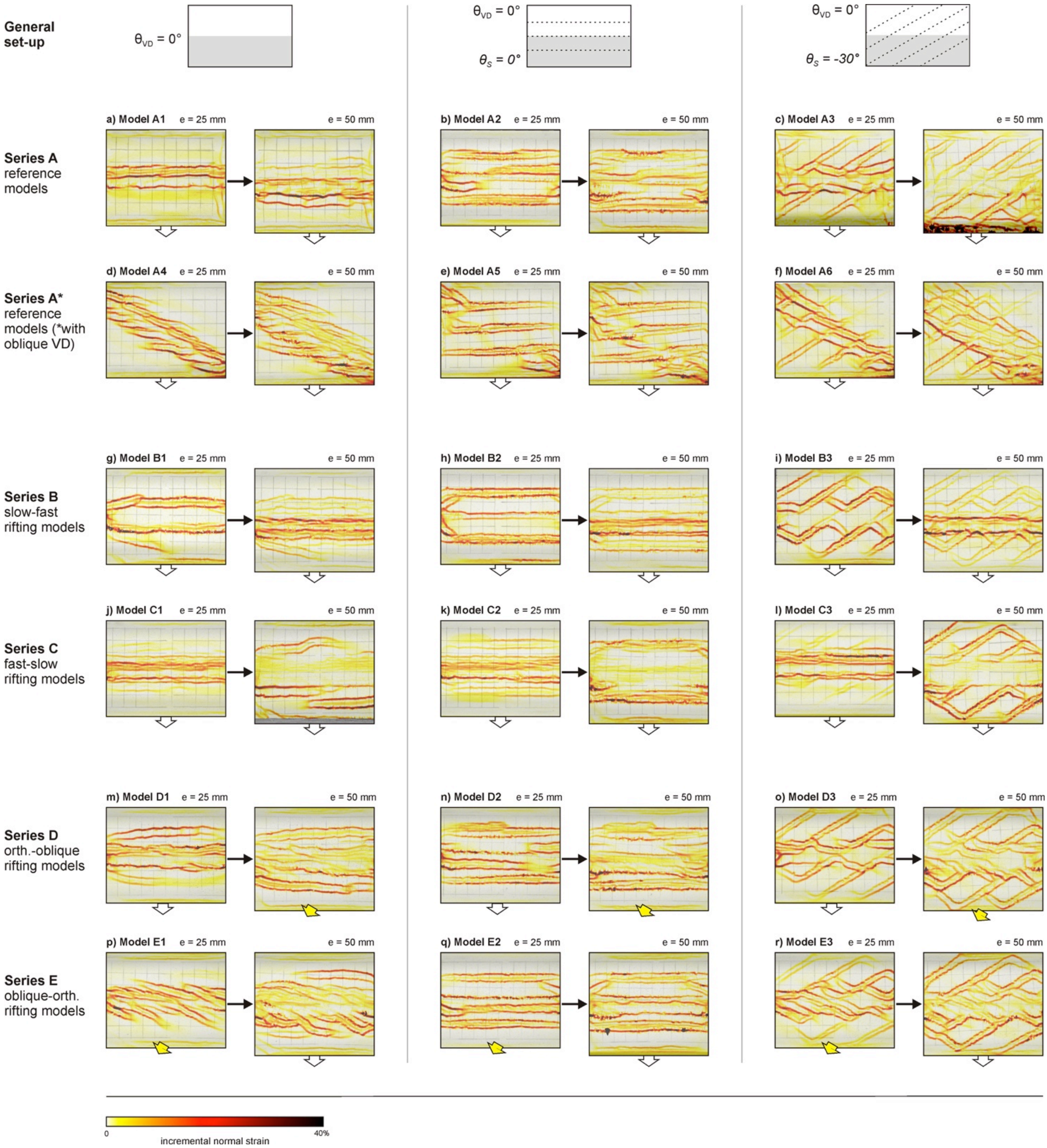

Fig. 7. Overview of maximum normal strain evolution of reference model Series A, and from multiphase rifting models (Series B-E) with a model axis-parallel VD (θ_{VD} = 0˚) that are representative of the influence of changes in divergence rate and direction. Divergence increments for PIV analysis were 5 mm. A complete overview of strain results is included in the Appendix (Fig. A1).

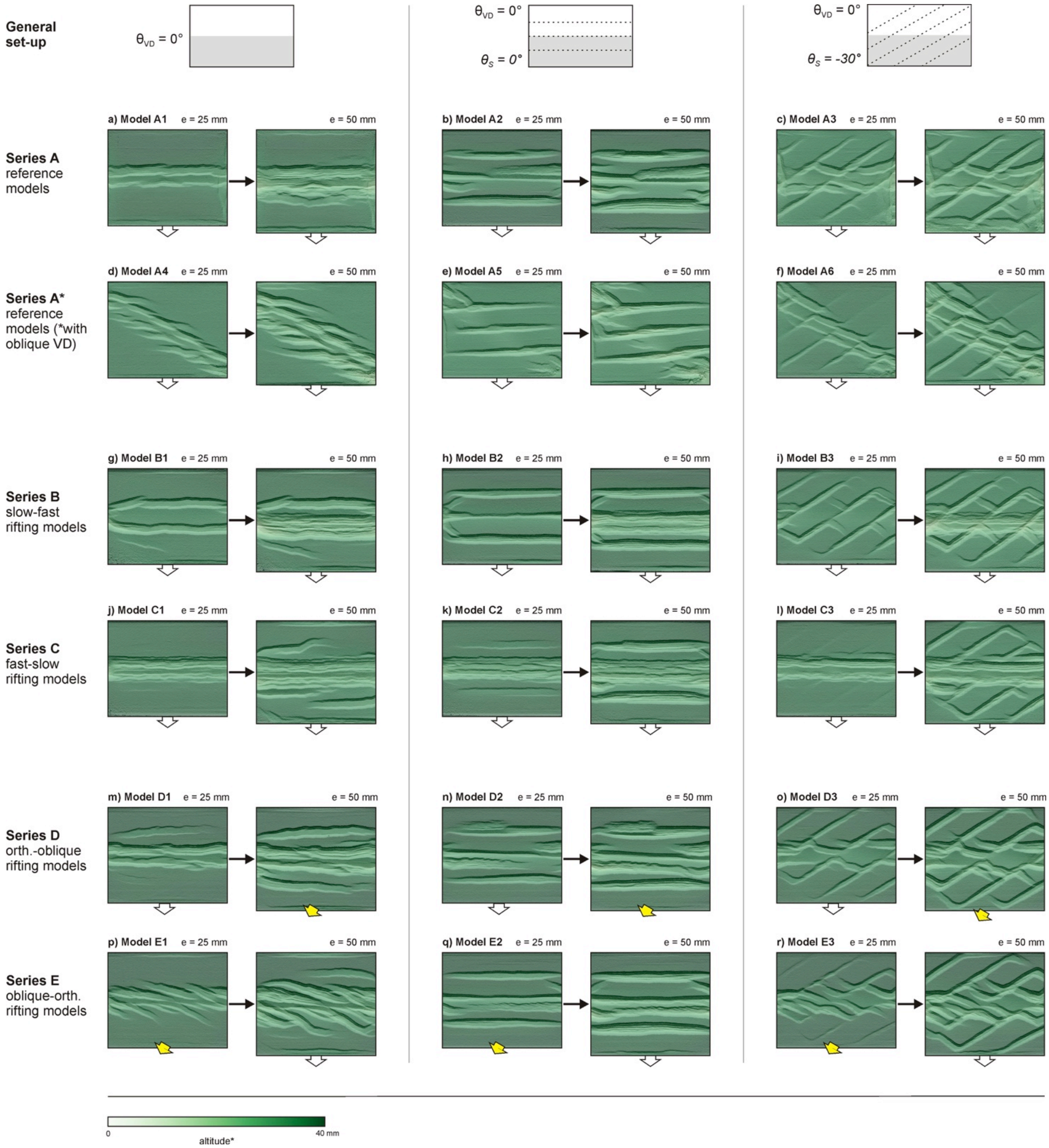

Fig. 8. Overview of topographic evolution of reference model Series A, and from multiphase rifting models (Series B-E) with a model axis-parallel VD (θ_{VD} = 0˚) that are representative of the influence of changes in divergence rate and direction. A complete overview of topography results is included in the Appendix (Fig. A2).

4.1.3. Effects of divergence direction variations

Finally, the results from model Series D and E show how changing divergence directions affected rift structures (Figs. 7m-r, 8m-r). Although there were some slight differences, the models from Series D, with an initial phase of orthogonal rifting created very similar structures as those in the early stages of the reference models (Figs. 7a-c, m-o, 8a-c, m-o). The second phase of oblique rifting did not significantly alter the well-established structural arrangement from the first orthogonal rifting phase, so that the final structures in these models of Series D were very similar to those of the Series A reference models (Fig. 8a-c, m-o). By contrast, Series E models showed clear deviations from the previous patterns (Figs. 7p-r, 8p-r), as Model E1 developed a series of en echelon grabens along the VD, similar to those found in reference Model A4 (Fig. 8d, 8e). Yet when seeds were present, these did localize significant amounts, if not most, of deformation and only minor details such as the orientation of VD-induced grabens would betray the occurrence of an initial phase of oblique rifting (Figs. 7q-r, 8q-r). Similar to the Series D models, a shift in divergence direction, here from oblique to orthogonal, did not significantly affect the subsequent rift evolution (Figs. 7m-r, 8m-r). Only when no seeds are present, a slight realignment of new faults towards the normal to the divergence direction occurs (Figs. 7p, 8p).

4.2. Comparison with previous analogue and numerical modelling studies

4.2.1. Reference models

Our reference model results are consistent with the observations from previous modelling studies. These earlier studies show that, without a seed, a double graben forms due to the presence of shallow-dipping shear zones originating from the VD or mantle discontinuity (e.g., Tron & Brun 1991; Michon & Merle 2000; 2003, Dyksterhuis et al. 2007; Zwaan et al. 2019; 2021a; Oliveira et al. *in review*) (Figs. 7a, 8a). The en echelon grabens developing along an oblique VD (Figs. 7d, 8d) are typical for such model set-ups, as the effective stretching direction is locally deviated by the oblique VD (e.g., Tron & Brun 1993; Bonini et al. 1997; Clifton et al. 2000; Van Wijk 2005; Morley 2010; Brune & Autin 2013; Ruh et al. 2019; Ducleaux et al. 2020; Reiter 2021; Zwaan et al. 2021a).

The varying effects of the simulated crustal weaknesses in our models are in agreement with previous model results. Models by e.g., McClay and White (1995), Bellahsen and Daniel (2005), Zwaan and Schreurs (2017), Deng et al. (2018), Molnar et al. (2019), Maestrelli et al. (2021), and references therein show that inherited weaknesses oriented obliquely to the divergence direction are less favourably oriented, and thus less likely to localize deformation. Conversely, weaknesses that are oriented orthogonally to the divergence direction are more likely to localize deformation during rifting. As a result of this geometrical rule, Zwaan et al. 2021a describe how simulated crustal and mantle weaknesses may compete during rifting, with one type of weakness dominating the system if oriented perpendicular to the divergence direction. This same process was clearly observed in our models and led to complex rift structures with different structural orientations forming during a single rift event (Figs. 7b, c, e, f, 8b, c, e, f).

4.2.2. Divergence rate effects

The general effects of divergence rates on rift evolution are complex and partially documented in previous modelling publications, but comparing our results to these previous publications also highlights some apparent paradoxes. Firstly, slow rifting in our models localized deformation along the simulated crustal weaknesses (Figs. 7h, i, k, l, 8h, I, k, l), as reported by e.g., Zwaan et al. (2016). On the other hand, the fast-rifting models strongly focus deformation along the VD instead (as hinted at by Zwaan et al. 2021a), which is however in contrast to the distributed deformation or (wide) rifting style due to high divergence rates described by e.g., Brun (1999), Nestola et al. (2015) and Zwaan et al. 2016). The key factor in this paradox is the basal model boundary condition (Zwaan et al. 2019): when a strong mantle with a (single) VD is simulated, and coupling is sufficiently high by means of a high divergence rate, or a strong (or thin) lower crustal layer, this VD will induce deformation in the upper crustal layer (Fig. 9b). However, if the simulated mantle stretches uniformly (e.g., by using a model set-up with a foam base or a rubber sheet), high coupling leads to dominant distributed deformation in the upper crustal layer (e.g., Schlagenhauf et al. 2008, Zwaan et al. 2019), even if seeds are present (Zwaan et al. 2016) (Fig. 9d). By contrast, low coupling due to slow rifting (or a weak or thick lower crust) is known to isolate the upper crustal layer from the simulated mantle, so that deformation is free to localize along heterogeneities within the upper crustal layer (e.g. Zwaan et al., 2019) (Fig. 9c). Moderate divergence rates in combination with a distributed deformation basal boundary condition leads to a hybrid deformation style, with both widespread faulting and localization along the seeds (Zwaan et al. 2016).

Although several works have addressed the general effects of divergence rates during rifting, little attention has been dedicated to the effects of changing divergence rates over time. To our knowledge, only Brun & Tron (1993) have applied such multiphase rifting in brittle-viscous models with a VD but no seeds. Their model results also indicate that initial high coupling due to high divergence rates localizes deformation along the VD, whereas subsequent lower divergence rates tend to distribute deformation over a broader zone along the VD, in line with our model results (Fig. 9b’). Furthermore, Brune et al. (2016) have numerically modelled increasing divergence rates through force-boundary conditions. Yet in these numerical models, the increase in divergence rate is the result of necking and weakening of the lithosphere allowing faster plate motion, whereas necking (or localization along the VD) in our models is the result of faster plate motion itself. Due to these differences in boundary conditions between our models and the study of Brune et al. (2016) a comparison is challenging, but the sequence of events is the same nevertheless (Fig. 9a).

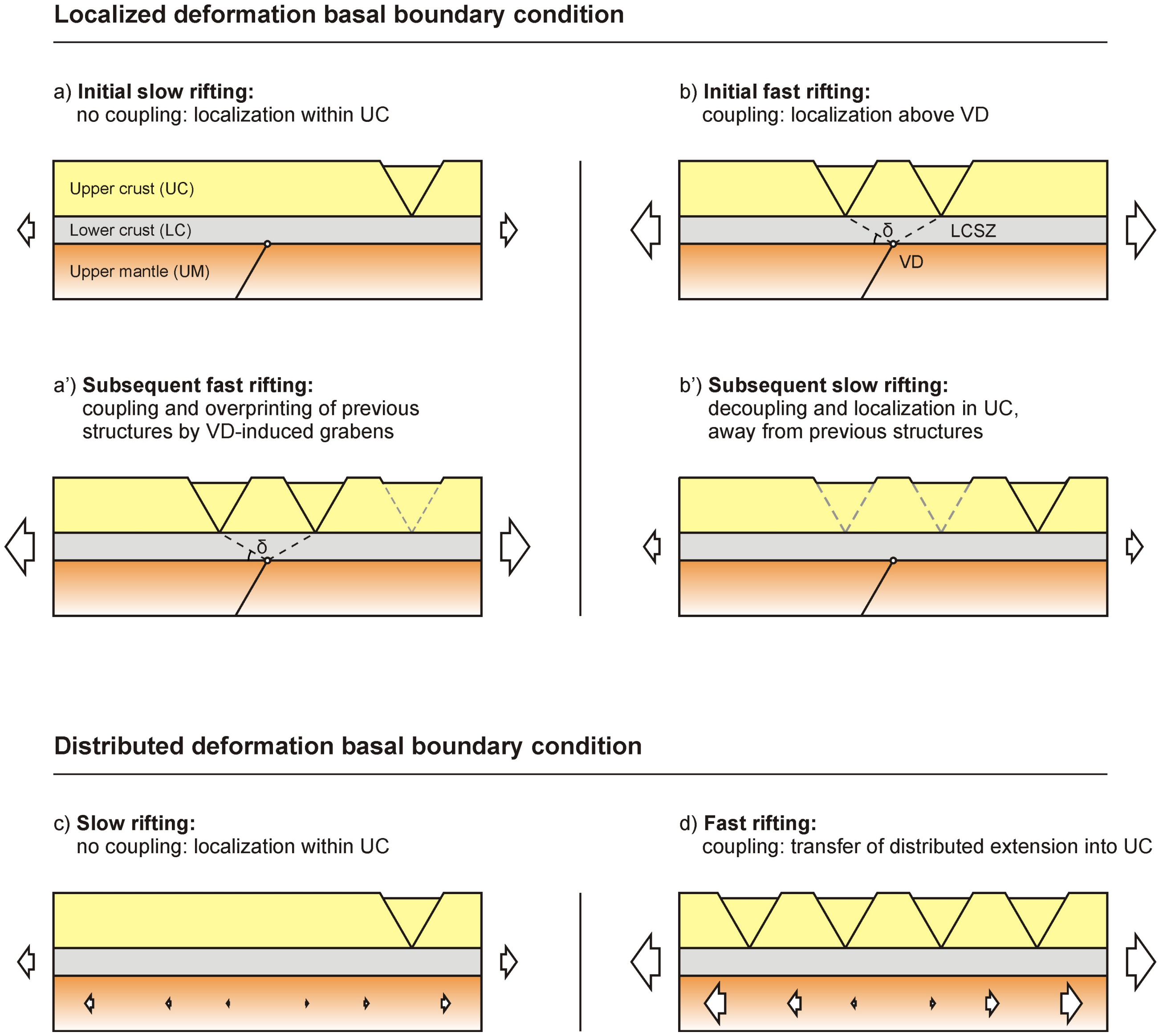

Fig. 9. General effects of divergence rates on rift evolution in brittle-viscous models. (a-b) Effects of changing divergence rates as observed in our models with a set-up simulating a strong lower crustal layer. (a) Slow rifting causes decoupling of the Upper crust (UC) and upper mantle (UM), leading to localization of faulting within the upper crust (UC), unaffected by any mantle weakness or velocity discontinuity (VD). (b) By contrast, fast rifting leads to coupling between the UC and UM, leading to localized rift development as deformation is transferred from the VD to the UC through lower crustal shear zones (LCSZ) with dip angle δ. (c-d) Expected effects of different divergence rates in models with a set-up involving a ductile upper mantle layer that distributes stretching. (c) Slow rifting causes decoupling of the UC from the UM, whereas (d) fast rifting leads to coupling and transfer of distributed deformation into the UC. Modified after Zwaan et al. (2019, 2021a).

4.2.3. Changing divergence direction

While the impact of changing divergence rates remains poorly explored in the literature, more attention has been dedicated to the effects of changing divergence directions. The general observation that structures developing during the first rifting phase are likely to control subsequent deformation phases involving a different divergence direction is also reported by Bonini et al. (1997), Bellahsen & Daniel (2005); Dubois et al. (2002); Henza et al. (2010, 2011), Withjack et al. (2017) and Wang et al. (2021). Interestingly, Virgo et al. (2014) made somewhat similar observations in their numerical models of small-scale fracture network development in changing stress fields. Yet, as pointed out by Henza et al. (2010; 2011) and Wang et al. (2021), the amount of deformation during the first rifting phase is a dominant factor. If only minor deformation occurred during this first phase, the resulting structures may not have sufficiently developed to localize subsequent deformation. A hint of this effect is visible in the Model E1 (and E4), where the new faults away from the central rift during the second phase did realign (Figs. 5d, 7p, 8p). This argument can also be made for pre-existing structures in general, whether resulting from an initial rifting phase or any other preceding tectonic phase (e.g., Zwaan et al. 2021a), and as discussed in section 4.2.1, also the direction of such structures with respect to the divergence direction is expected to have an important influence on whether these inherited structures will reactivate or not.

4.2.4. Relations between factors affecting rifting

Although our model results show that divergence, affecting the degree of coupling between the upper crust and upper mantle, is a key parameter affecting early rift evolution, we must consider a wider variety of parameters to get a better grasp of what factors control the evolution of continental rift systems. By combining observations from our models and from previous brittle-viscous modelling studies, we drafted a more general overview of these factors and their relative importance, that can serve as a “recipe” for assessing rift evolution (Fig. 10):

- As pointed out in a similar graph in the review paper by Corti et al. (2003), and by Zwaan et al. (2019) and Zwaan & Schreurs (2021), the structure of the lithosphere, i.e., the presence and thickness of the ductile lower crust, is a key factor. In the absence of such a layer, deformation is fully controlled by the mantle. Such mantle-controlled deformation in the crust can be either localized or distributed (e.g., Zwaan et al. 2019). By contrast, a very thick weak lower crustal layer fully decouples the crust from the underlying mantle, so that the upper crust is free to deform independently from the mantle.

- Divergence rates become an important factor when the weak lower crustal layer is of moderate thickness, since its rheology is strain-rate dependent. As such, fast rifting tends to strengthen the lower crustal layer, leading to increased coupling between the upper mantle and upper crust so that the mantle will have more control on deformation in the upper crust. By contrast, when rifting is slow, the lower crustal layer will remain weaker, leading to decoupling and less influence of the underlying mantle.

- When strong coupling between the upper mantle and upper crust occurs due to fast rifting, the deformation in the upper mantle determines what type of deformation is induced in the upper crust. In case of a stable continental lithosphere, we expect a strong upper mantle (e.g., Brun 1999), a fracture or shear zone in which would subsequently strongly localize deformation in the overlying crust (e.g. Oliveira et al. *in review*, Fig. 9b). The orientation of the mantle weakness with respect to the divergence direction then determines what kind of faulting will form within the localized rift zone in the upper crustal layer. Yet when the lower crust behaves in a more ductile fashion, involving more distributed deformation, we would expect this distributed deformation to be overprinted onto the upper crust (e.g. Zwaan et al. 2016), and the faulting in the upper crustal layer to be generally oriented (sub-) perpendicular to the divergence direction. Note that these general effects would also occur in a highly coupled system without a weak lower crustal layer.

- However, if coupling between the upper mantle and upper crust remains low due to slow rifting, we may expect that deformation in the upper crust will be dominated by pre-existing weaknesses from previous tectonic phases (including a potential initial rifting phase), if such weaknesses are present. How well these weaknesses will localize deformation depends on to what degree they weaken the upper crust, and how they are oriented to the divergence direction (orthogonal weaknesses react best, oblique weaknesses much less so) (Bellahsen & Daniel 2005; Henza et al. 2010, 2011; Wang et al. 2021, Zwaan et al. 2021a). If different orientations of crustal weaknesses are present, subsequent rift arrangements are expected to be complex (e.g., Maestrelli et al. 2021). Note that these same effects should also occur in a system with a very thick lower crustal layer causing decoupling between the upper crustal and mantle layers.

- In the case of moderate coupling between the upper mantle and upper crust, we expect that both the mantle (either deforming in a localized or distributed fashion) and weaknesses in the crust will affect subsequent rifting. These rift structures have been shown to be the most intricate as the controlling factors in both lithospheric layers will interact and compete (Molnar et al. 2020; Zwaan et al. 2021a, this study). Similar to the low-coupling case, the orientation of mantle- and crustal weaknesses to the divergence direction is of great importance, defining which factor will best localize deformation. Yet distributed deformation in the mantle may lead to a degree of regional background overprinting by distributed deformation (Zwaan et al. 2016).

Note that Fig. 10 classifies the different types of deformation related to the various factors during a single rift phase. When assessing rift systems involving multiple rift phases with different divergence velocities or directions, the diagram can be used in a serial fashion, each time starting from the top.

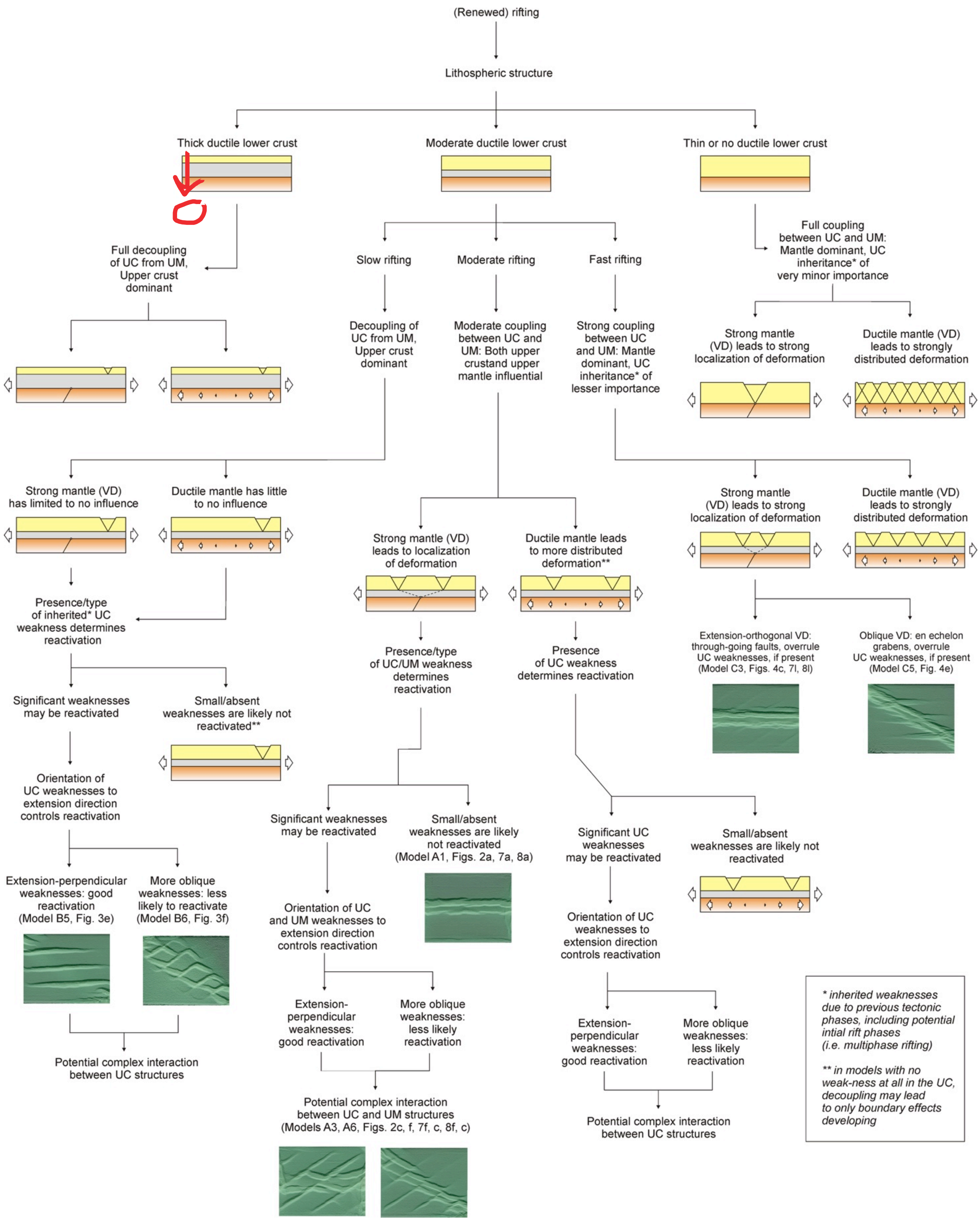

Fig. 10. Flow diagram with the relations between the various factors affecting continental rift evolution, based on brittle-viscous models from this study and previous models. Sections illustrate 2D effects and are oriented in the direction of divergence, whereas maps show more complex 3D effects, where appropriate. UC: upper crust, UM: upper mantle, VD: velocity discontinuity. For legend see Figs. 8 and 9. Note that, although the flow chart does not elaborate on the thick and absent weak lower crust scenarios (i.e. full decoupling and full coupling, respectively), we should expect very similar influences of the mantle and crustal weaknesses to those described for the moderate lower crust settings

with slow and fast extension (i.e. decoupling and strong coupling), respectively. See text (section 4.2.4) for details.

4.3. Model strengths and limitations

Although our models provide valuable insights into the effects of inherited weaknesses and multiphase rifting on rift systems, our models have some limitations that need to be taken into account when extrapolating their results. Firstly, our simple model set-up, did not allow us to model beyond the initial stages of continental rifting and the subsequent necking phase: none of the processes related to continental break-up and oceanic spreading processes could be simulated. Indeed, even though we do assume a specific mantle boundary condition (Zwaan et al. 2019), no thermal effects, magmatic activity or isostatic compensation induced by the rising sub-lithospheric mantle were included in our models. This is however an acceptable limitation since these factors are not considered to be of great importance during the early evolution of magma-poor rift systems (stretching to onset of necking) we aimed to simulate (Chenin et al. 2019b; 2020). Magma-rich rifts may have a very different evolution since magmatism can strongly localize deformation early on during rifting (e.g., Ebinger 2005; Buck 2004, 2006; Zwaan et al. 2020a). The lack of syn-rift sedimentation, that can also have a significant impact on rift evolution by loading and thermal blanketing (e.g., Burov & Cloetingh 1997; Buiter et al. 2008; Bialas & Buck 2009; Martín-Barajas et al. 2013) was not a major issue due to the limited amounts of accommodation space being generated in these early stages of rifting (Zwaan et al. 2018a). In fact, the relative simplicity of our model set-up is an advantage, as it allowed us to clearly identify the effects of specific parameters on rift evolution (Figs. 7, 8). A final "limitation" is the fact that large parts of the vast parameter space in terms of divergence directions, rates and styles (e.g., symmetric vs. asymmetric, Allemand & Brun 1991), as well as structural inheritance (different types, orientations, combinations and arrangements) and many other factors ranging from differences in general lithospheric rheology to surface processes, remains unexplored in this work. This could hardly have been otherwise for practical reasons, but the possibilities provide a strong incentive for future modelling efforts (Zwaan & Schreurs 2021). Within the context of this study, an especially interesting point of attention could be the application of force- rather than divergence rate (i.e., velocity) boundary conditions that are so important according to Brune et al. (2016).

4.4. Implications for interpreting natural rift systems

Our model results have a number of implications for the interpretation of natural rift systems developing in a stable, thermally equilibrated continental lithosphere with a strong upper crustal and upper mantle layer. Firstly, the complex structures as a result of the interaction and competition between mantle and crustal weaknesses in our reference models from Series A (Figs. 7a-f, 8a-f) highlight the suggestion by Reeve et al. (2015) and Zwaan et al. (2021a) that complex rift structures with multiple structural orientations can be formed during a single phase of rifting. As such, when encountering such rift arrangements in the field, as for instance in the North Sea (Erratt et al. 1999; 2010 and references therein), there is no direct need to invoke changes in the divergence direction over time, and divergence was also not necessarily (sub-)orthogonal to either of the normal faults.

However, when changes in divergence rate occur, it can have significant impacts on rift evolution. A shift from slow to fast rifting in our Series B models, as is characteristic for lithospheric necking (Brune et al. 2016) is expected to be associated with a strong localization of deformation (Fig. 7g-i, 8g-i). In this case, the mantle becomes the dominant factor and any previous structures controlled by crustal weaknesses may diminish or cease to be active (Chenin & Beaumont, 2013; Chenin et al. 2019b, Fig. 9a, a'). Such an increase in divergence rate could perhaps explain the overprinting of the Late Jurassic grain by an Early Cretaceous fabric in the North Sea (Erratt et al. 1999). Whether the acceleration of rifting is due to the necking itself while external forces remain constant as suggested by Brune (2016), or whether it can be a result of increasing external forces such as subduction-induced drag on the plates remains an open question. Importantly, a strongly localized but waning rift system as in our Series C models (Figs. 7j-l, 8j-l), might shift to a more distributed deformation style, where upper crustal weaknesses may reactivate as the upper crust becomes decoupled from the mantle (Fig. 9b, b'. Similar to the reference models, the rift patterns in these models can be very complex and can strongly overprint each other, so that the resulting final structures may be very similar.

The results from our models with changing divergence directions suggest that structures formed during an initial phase of rifting will strongly control the localization of deformation during a subsequent rift phase that involves a different divergence direction. A good example of such changing divergence directions reactivating rift structures from a previous phase is the Afar Rift in East Africa (Chorowicz et al. 1999; Zwaan et al. 2020b, c). Yet, as observed in other models, and in the Turkana Depression in East Africa, a previous minor rifting phase may not build impactful structures to significantly control where subsequent deformation localizes (Henza et al. 2010, 2011; Wang et al. 2021). Therefore, when changes in divergence direction are suspected in a natural rift system, careful examination is needed to determine whether the different structural directions did indeed develop during subsequent rift phases, instead of being the result of a complex structural inheritance.

Indeed, careful examination by combining information from different sources is the key to better assess the evolution of natural rift systems. Structural field studies provide important insights (e.g. Chorowicz et al. 1999; Samsu et al. 2019; Zwaan et al. 2020c), but particular attention should be dedicated to detailed fault activity analysis through seismic interpretation (e.g. Erratt et al. 1999; Bell et al. 2014; Claringbould et al. 2017, 2020, Phillips et al. 2019). Such fault analyses address the distribution of rift depocenters, their syn-rift sedimentary infill and their relation to faulting, which provides key insights into rift development. Yet an important caveat, as pointed out by Erratt et al. (1999) and Chenin et al. (2015), is that rift basins may experience very limited syn-rift deposition when the system is approaching the necking stage, leading to a "necking unconformity" (e.g. the Base Cretaceous Unconformity in the North Sea, Chenin et al. 2015), as post-rift deposits start filling in these previously sediment-starved basins. As a result, syn-rift deposits may only provide a limited record of rift development and the post-rift deposits can capture important changes in rift structure and depocenter distribution that are not recorded by (late) syn-rift units. Thus, only by incorporating information from the analysis of both syn-rift and post-rift infill, provides a more complete overview of rift evolution can be established. Such overviews could subsequently be compared to our model results and our flow diagram, in order to identify what factors might have been at play during rifting (Figs. 7, 8, 10, A1, A2).

5. Conclusion

In this paper we presented an analogue modelling study involving brittle-viscous set-ups to study how multiphase rifting (changes in divergence rate or –direction) in a continental lithosphere containing pre-existing weaknesses in the competent mantle and crust may affect the evolution of a rift system. By examining our model results we came to the following conclusions:

- Complex rift structures can be the result of reactivation of weaknesses in both the mantle and crust during a single phase of rifting involving moderate divergence rates (i.e., moderate coupling between the mantle and upper crustal layers), without the need to invoke changes in divergence direction over time. The relative importance of these weaknesses is then a function of their impact on the strength of the layer they are situated in, as well as their orientation with respect to the divergence direction.

- Changing the divergence rate and associated mantle-crustal coupling strongly affects the localization of deformation. Slow rifting in lithosphere where crust-mantle coupling is weak favours surficial expression of shallow (crustal) weaknesses with respect to weaknesses located in the mantle. Conversely, fast rifting causes strong coupling and a dominance of mantle weaknesses leading to significant localization of deformation. A shift from slow to fast rifting causes strong localization along the mantle VD and overprinting of any previous structures controlled by the crustal weaknesses. Conversely, a shift from fast to slow rifting leads to delocalization and a reactivation of crustal weakness-induced structures. Yet the final structures obtained through either shift can be very similar.

- In rift systems that undergo changes in divergence directions, the structures from the first rifting phase may strongly control where subsequent deformation takes place. Yet when these first phase structures are only poorly developed, they will likely not have a significant effect on subsequent rifting, which may simply ignore these pre-existing weaknesses and create a wholly new structural orientation. Therefore, the final result can vary greatly, depending on the magnitude and direction of divergence during the initial rifting phase.

  Placed in a larger framework of brittle-viscous modelling results from previous studies, we obtain useful insights into the relative importance of the various internal and external factors affecting rift evolution. It follows that the structure of the lithosphere is the most important parameter, followed by divergence rate, the type of deformation in the lithospheric mantle and finally structural inheritance in the upper crust. Within this framework, the interaction between these various factors in 3D and over time can lead to a large variety of deformation styles.

- Altogether, our model results highlight that rift evolution may be strongly affected by structural inheritance in both the crust and the mantle and by changes in divergence rate (and to a lesser degree by changes in divergence direction and the amount of divergence), often, but not always, leading to very similar end products. Therefore, detailed investigation of fault activity and to an equal degree basin depocenter distribution over time (including the distribution of both syn- and post-rift strata) is needed to properly determine the structural history of complex rift systems. These insights, summarized in our overview figures and flow chart (Figs.

7, 8, 10, A1, A2) provide a strong incentive to revisit the current interpretation of various natural examples.

Data availability

Images and videos of the models, including PIV analyses results, are freely available in the shape of a data publication stored on the GFZ Data Services database (Zwaan et al., 2021b). Link: XXX TO BE CREATED XXX

Temporary link:
https://www.dropbox.com/sh/ousqc4hqyq5nd5p/AACB9hpYnx-8ww0EdpjUsI6ma?dl=0

Author contribution

FZ: Conceptualization, Formal analysis, Investigation, Methodology, Validation, Visualization, Writing – original draft preparation
PC: Conceptualization, Methodology, Writing – review & Editing
DE: Conceptualization, Methodology, Writing – review & Editing
GM: Conceptualization, Methodology, Resources, Writing – review & Editing
GS: Conceptualization, Methodology, Funding acquisition, Resources, Writing – review & Editing

Competing interests

The authors declare that they have no conflict of interest

Acknowledgements

We thank Timothy Schmid, Michael Rudolf, Matthias Rosenau, and the software engineers from LaVision (Dave Hollis, Horst Nagel, Torsten Siebert) for technical support during the PIV analysis in DaVis. We would also like to thank Kirsten Elger for helping us creating the GFZ data publication with the supplementary material (Zwaan et al. 2021b). This research was funded by the Swiss National Science Foundation (grant 200021-178731, http://p3.snf.ch/Project-178731), and Open Access publication costs were covered by the University of Bern.

Appendix A

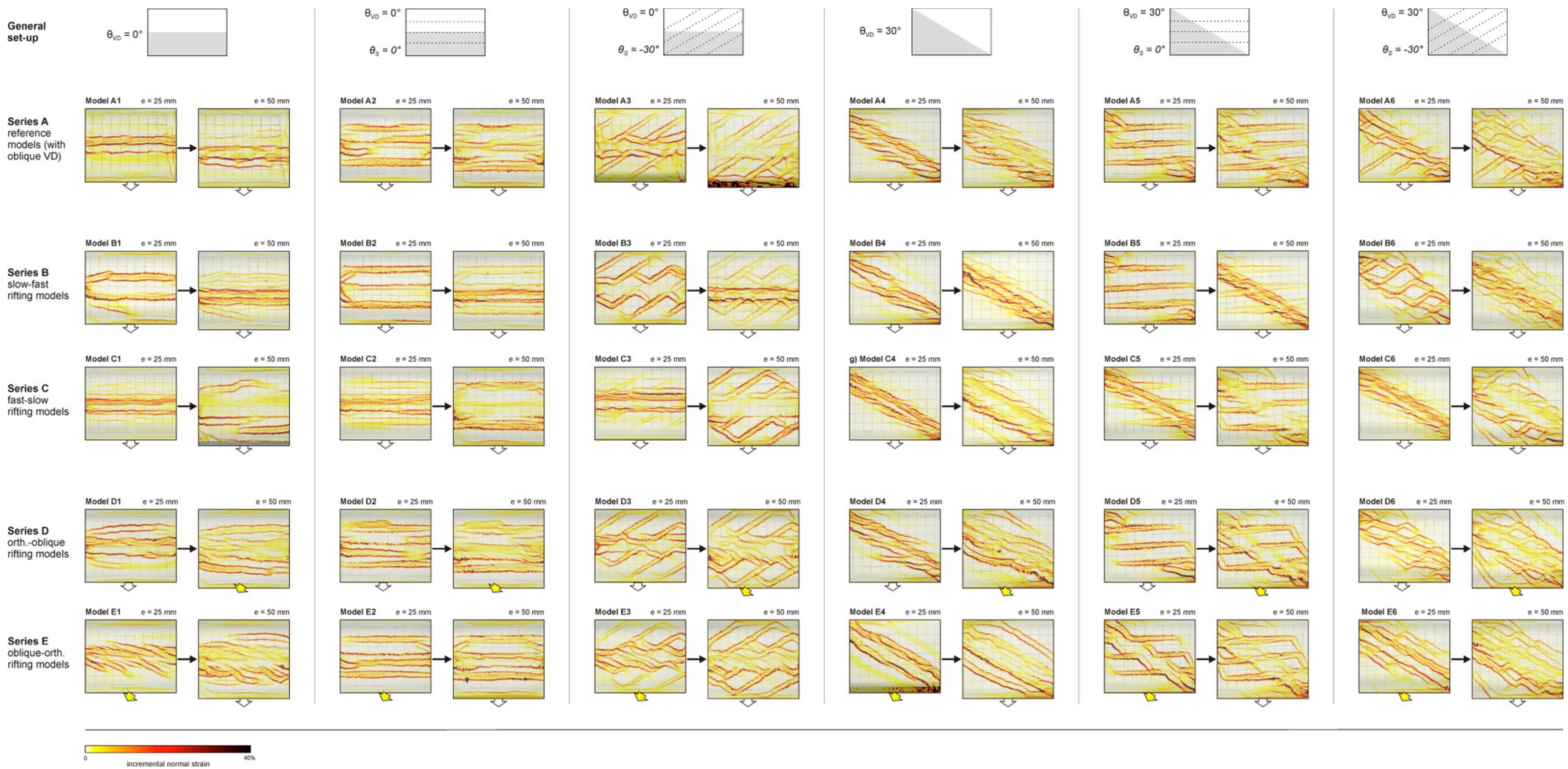

Fig. A1. Complete overview of the strain evolution of the models presented in this paper. Each panel depicts the maximum normal strain of the models after 25 mm or 50 mm of divergence, calculated over a preceding 5 mm increment of divergence.

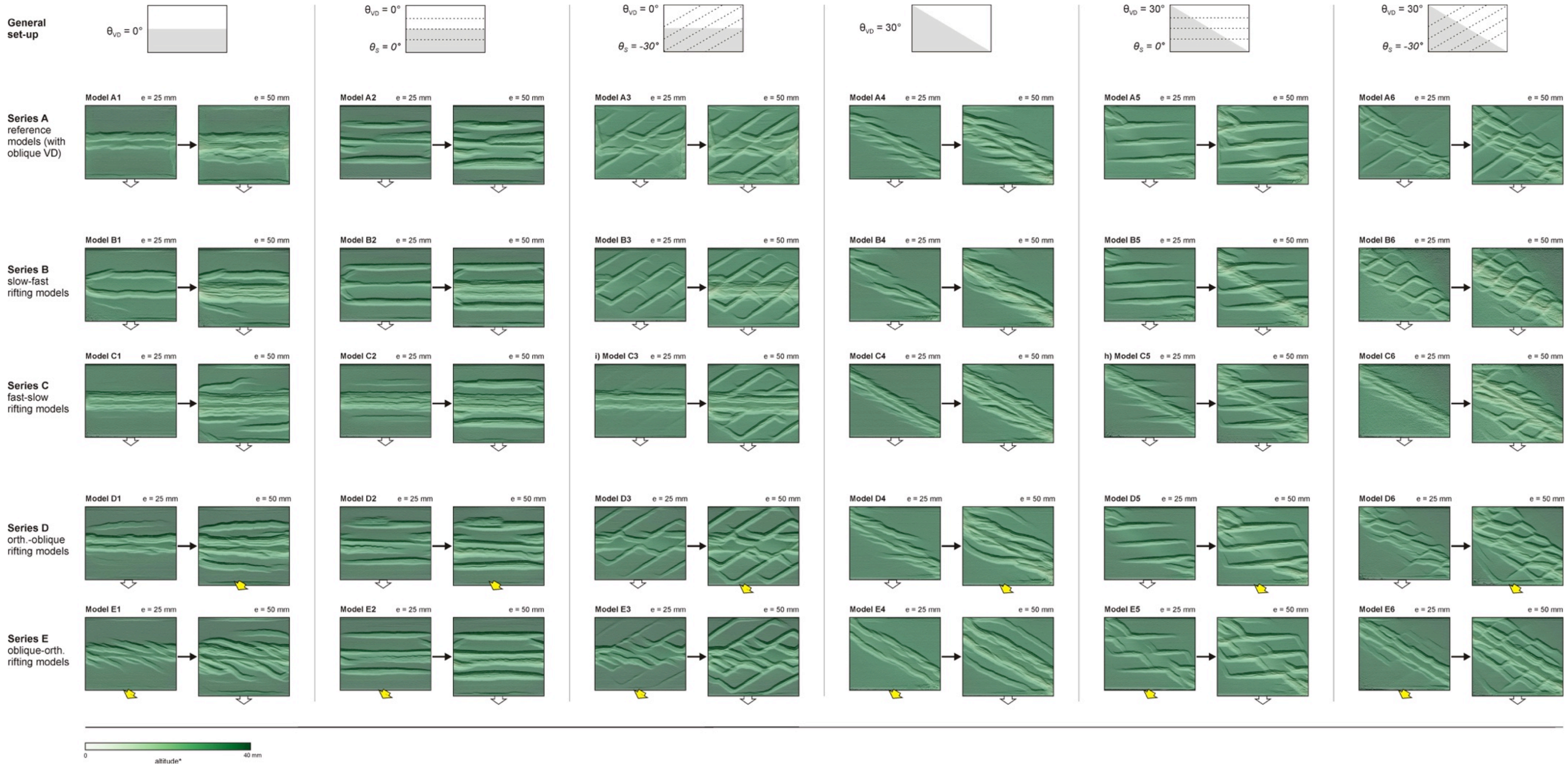

Fig. A2. Complete overview of topographic evolution of the models presented in this paper.

References

Adam, J., Urai, J.L., Wieneke, B., Oncken, O., Pfeiffer, K., Kukowski, N., Lohrmann, J., Hoth, S., Van der Zee, W., Schmatz, J., 2005. Shear localisation and strain distribution during tectonic faulting—new insights from granular-flow experiments and high-resolution optical image correlation techniques, J. Struct. Geol., 27, 283-301. https://doi.org/10.1016/j.jsg.2004.08.008

Agostini, A., Corti. G., Zeoli, A., and Mulugeta, G. , 2009. Evolution, pattern, and partitioning of deformation during oblique continental rifting: Inferences from lithospheric-scale centrifuge models, Geochem. Geophy. Geosy., 10, Q11015. https://doi.org/10.1029/2009GC002676

Allemand, P., Brun, J.-P., 1991. Width of continental rifts and rheological layering of the lithosphere, Tectonophysics, 27, 283-301. https://doi.org/10.1016/0040-1951(91)90314-I

Autin, J., Bellahsen, N., Husson, L., Beslier, M.-O., Leroy, S., d'Acremont, E., 2010. Analog models of oblique rifting in a cold lithosphere, Tectonics 29, TC6016. https://doi.org/10.1029/2010TC002671

Autin, J., Bellahsen, N., Leroy, S., Husson, L., Beslier, M.-O., d'Acremont, E., 2013.The role of structural inheritance in oblique rifting: Insights from analogue models and application to the Gulf of Aden, Tectonophysics 607, 51-64. http://dx.doi.org/10.1016/j.tecto.2013.05.041

Bell, R.E., Jackson, C.A-L., Whipp, P.S., and Clements, B., 2014. Strain migration during multiphase extension: observations from the northern North Sea, Tectonics 33, 1936–1963. https://doi.org/10.1002/2014TC003551

Bellahsen, N., Daniel, J.M., 2005. Fault reactivation control on normal fault growth: an experimental study, J. Struct. Geol., 27, 769-780. https://doi.org/10.1016/j.jsg.2004.12.003

Bialas, R.W., Buck, W.R., 2009. How sediment promotes narrow rifting: applications to the Gulf of California. Tectonics 28, TC4014. https://doi.org/10.1029/2008TC002394.

Bonini, M., Souriot, T., Boccaletti, M., Brun, J.-P., 1997. Successive orthogonal and oblique extension periods in a rift zone: Laboratory experiments with application to the Ethiopian Rift, Tectonics, 16, 347-362. https://doi.org/10.1029/96TC03935

Boutelier, D., Schrank, C., Regenauer-Lieb, K., 2019. 2-D finite displacements and strain from particle imaging velocimetry (PIV) analysis of tectonic analogue models with TecPIV, Solid Earth, 10, 1123–1139. https://doi.org/10.5194/se-10-1123-2019

Brun, J.-P., 1999. Narrow rifts versus wide rifts: inferences for the mechanics of rifting from laboratory experiments, Philos. T. R. Soc. A, 357, 695–712. https://doi.org/10.1098/rsta.1999.0349

Brun, J.-P., Tron, V., 1993. Development of the North Viking Graben: inferences from laboratory modelling, Sediment. Geol., 86, 31-51. https://doi.org/10.1016/0037-0738(93)90132-O

Brune, S., Autin. J., 2013. The rift to break-up evolution of the Gulf of Aden: Insights from 3D numerical lithospheric-scale modelling, Tectonophysics 607, 65-79. http://dx.doi.org/10.1016/j.tecto.2013.06.029

Brune, S., Williams, S.E., Butterworth, N.P., and Müller, R.M., 2016 Abrupt plate accelerations shape rifted continental margins, Nature 536, 201-204. https://doi.org/10.1038/nature18319

Buiter, S.J.H., Huismans, R.S., Beaumont, C. 2008. Dissipation analysis as a guide to mode selection during crustal extension and implications for the styles of sedimentary basins. J. Geophys. Res. 113, B06406. https://doi.org/10.1029/2007JB005272

Buck, W.R., 2004. Consequences of asthenospheric variability on continental rifting. In: Karner, G.D., Taylor, B., Droscoll, N.W., Kohlstedt, D.L. (Eds.), Rheology and Deformation of the Lithosphere at Continental Margins. Columbia Univ. Press, New York, pp. 1–30. https://doi.org/10.7312/karn12738-002

Buck, W.R., 2006. The role of magma in the development of the Afro-Arabian Rift System. In: Yirgu, G., Ebinger, C.J., Maguire, P.K.H. (Eds.), The Afar Volcanic Province within the East African Rift System 259. Geol. Soc. Spec. Publ., pp. 43–54. https://doi.org/10.1144/GSL.SP.2006.259.01.05

Buck, W.R., 1991. Models of Continental Lithospheric Extension, J. Geophys. Res., 96, 20,161-20,178. https://doi.org/10.1029/91JB01485

Burov, E.B., 2011. Rheology and strength of the lithosphere, Mar. Petr. Geol., 28, 1402-1443. https://doi.org/10.1016/j.marpetgeo.2011.05.008

Burov, E., Cloetingh, S. 1997. Erosion and rift dynamics: new thermomechanical aspects of post-rift evolution of extensional basins. Earth and Planetary Science letters 150, 7-26. https://doi.org/10.1016/S0012-821X(97)00069-1

Burov, E.B., Watts, A.B., 2006. The long-term strength of continental lithosphere: “jelly sandwich” or “crème brûlée”? GSA Today 16. https://doi.org/10.1130/1052-5173(2006)016<4:tltSOc>2.0.cO;2

Byerlee, J., 1978. Friction of Rocks, Pure Appl. Geophys., 116, 615-626. https://doi.org/10.1007/BF00876528

Carlo AG (Carlo Bernasconi AG webpage): https://www.carloag.ch, last access: 6 July 2021

Chenin, P., Beaumont, C., 2013. Influence of offset weak zones on the development of rift basins: Activation and abandonment during continental extension and breakup, J. Geophys. Res-Sol. Ea., 118, 1698-1720, https://doi.org/10.1002/jgrb.50138

Chenin, P., Manatschal, G., Lavier, L.L., Erratt, D., 2015. Assessing the impact of orogenic inheritance on the architecture, timing and magmatic budget of the North Atlantic rift system: a mapping approach. J. Geol. Soc. 172, 711-720. https://doi.org/10.1144/jgs2014-139

Chenin, P., James, S., Lavier, L.L., Manatschal, G., Picazo, S., Müntener, O., Karner, G.D., Figueredo, P.H., Johnson, C., 2019a. Impact of mafic underplating and mantle depletion on subsequent rifting: A numerical modeling study, Tectonics 38, 2185–2207. https://doi.org/10.1029/2018TC005318

Chenin, P., Manatschal, G., Decarlis, A., Schmalholz, S.M., Duretz, T., Beltrando, M., 2019b. Emersion of distal domains in advanced stages of continental rifting explained by asynchronous crust and mantle necking. Geochem. Geophys. Geosyst. 20, 3821–3840. https://doi.org/10.1029/2019GC008357

Chenin, P., Schmalholz, S.M., Manatschal, G., Duretz, T., 2020. Impact of crust–mantle mechanical coupling on the topographic and thermal evolutions during the necking phase of 'magma-poor' and 'sediment-starved' rift systems: A numerical modeling study. Tectonophysics 786, 228472. https://doi.org/10.1016/j.tecto.2020.228472

Chorowicz, J., Collet, B., Bonavia, F., Korme, T., 1999. Left-lateral strike-slip tectonics and gravity induced individualisation of wide continental blocks in the western Afar margin. Eclogae Geol. Helv. 92, 149–158. https://doi.org/10.5169/seals-168656.

Claringbould, J.S., Bell, R.E., Jackson, C.A.-L., Gawthorpe, R.L., Odinsen, T., 2017. Pre-existing normal faults have limited control on the rift geometry of the northern North Sea, Earth Planet. Sc. Lett. 475, 190-206. http://dx.doi.org/10.1016/j.epsl.2017.07.014

Claringbould, J. S., Bell, R. E., Jackson, C. A.-L., Gawthorpe, R. L., Odinsen, T., 2020. Pre-breakup extension in the northern North Sea defined by complex strain partitioning and heterogeneous extension rates, Tectonics 39, e2019TC005924. https://doi.org/10.1029/2019TC005924

Clifton, A.E., Schlische, R.W., Withjack, M.O., Ackermann, R.V., 2000.Influence of rift obliquity on fault-population systematics: results of experimental clay models, J. Struct. Geol., 22, 1491-1509. https://doi.org/10.1016/S0191-8141(00)00043-2

Corti, G., 2012. Evolution and characteristics of continental rifting: Analog modeling-inspired view and comparison with examples from the East African Rift System, Tectonophysics 522-523, 1-33. https://doi.org/10.1016/j.tecto.2011.06.010

Corti, G., Bonini, B., Conticelli, S., Innocenti, F., Manetti P., Sokoutis, D., 2003. Analogue modelling of continental extension: a review focused on the relations between the patterns of deformation and the presence of magma, Earth-Sci. Rev., 63, 169–247. https://doi.org/10.1016/S0012-8252(03)00035-7

Corti, G., Philippon, M., Sani, F., Keir, D., Kidane, T., 2013. Re-orientation of the extension direction and pure extensional faulting at oblique rift margins: comparison between the Main Ethiopian Rift and laboratory experiments, Terra Nova 0, 1-9. https://doi.org/10.1111/ter.12049

Dauteuil, O., Bourgeois, O., Mauduit, T., 2002. Lithosphere strength controls oceanic transform zone structure: insights from analogue models, Geophys. J. Int., 150, 706-714. https://doi.org/10.1046/j.1365-246X.2002.01736.x

Deng, C., Gawthorpe, R. L., Fossen, H., Finch, E. , 2018. How does the orientation of a preexisting basement weakness influence fault development during renewed rifting? Insights from three-dimensional discrete element modeling, Tectonics, 37, 2221–2242. https://doi.org/10.1029/2017TC004776

Dubois, A., Odonne, F., Massonnat, G., Lebourg, T., Fabre, R. 2002. Analogue modelling of fault reactivation: tectonic inversion and oblique remobilisation of grabens. J. Struct. Geol. 24, 1741-1752. https://doi.org/10.1016/S0191-8141(01)00129-8

Duclaux, G., Huismans, R.S., May, D.A., 2020. Rotation, narrowing, and preferential reactivation of brittle structures during oblique rifting, Earth Planet. Sc. Lett., 531, 115952. https://doi.org/10.1016/j.epsl.2019.115952

Dyksterhuis, S., Rey, P., Müller, R.D., Moresi, L., 2007. Effects of initial weakness on rift architecture, Geol. Soc. Sp. 282, 443-455. https://doi.org/10.1144/SP282.18

Ebinger, C. 2005. Continental break-up: The East African perspective. *Astron. Geophys.* 46, 2.16–2.21. https://doi.org/10.1111/j.1468-4004.2005.46216.x

Erratt, D., Thomas, G.M., Hartley, N.R., Musum, R., Nicholson, P.H., Spisto, Y., 2010. North Sea hydrocarbon systems: some aspects of our evolving insights into a classic hydrocarbon province, Geological Society, London, Petroleum Geology Conference Series, 7, 37-56. https://doi.org/10.1144/0070037

Erratt, D., Thomas, G.M., Wall, G.R.T., 1999. The evolution of the Central North Sea Rift, Geological Society, London, Petroleum Geology Conference Series 5, 63-82. https://doi.org/10.1144/0050063

Handin, J., 1969. On the Coulomb-Mohr Failure Criterion, J. Geophys. Res., 74, 5343-5348, https://doi.org/10.1029/JB074i022p05343

Henza, A.A., Withjack, M.O., Schlische, R.W., 2010. Normal-fault development during two phases of non-coaxial extension: An experimental study, J. Struct. Geol. 32, 1656-1667, https://doi.org/10.1016/j.jsg.2009.07.007

Henza, A.A., Withjack, M.O., Schlische, R.W., 2011. How do the properties of a pre-existing normal-fault population influence fault development during a subsequent phase of extension? J. Struct. Geol. 33, 1312-1324. https://doi.org/10.1016/j.jsg.2011.06.010

Heron, P. J., Peace, A. L., McCaffrey, K. J. W., Welford, J. K., Wilson, R., van Hunen, J., Pysklywec, R.N., 2019. Segmentation of Rifts Through Structural Inheritance: Creation of the Davis Strait, *Tectonics*, *38*, 2411–2430. https://doi.org/10.1029/2019TC005578

Hubbert, M.K., 1937. Theory of scale models as applied to the study of geologic structures, Geol. Soc. Am. Bull., 48, 1459-1520. https://doi.org/10.1130/GSAB-48-1459

Jaeger, J.C., Cook, N.G.W., 1979. Fundamentals of Rock Mechanics. Chapman & Hall, Wiley, New York, United States of America. https://doi.org/10.1017/S0016756800044897

Keep, M., McClay, K.R. 1997. Analogue modelling of multiphase rift systems. Tectonophysics 273, 239-270. https://doi.org/10.1016/S0040-1951(96)00272-7

Kettermann, M., von Hagke, C., van Gent, H.W., Grützner, C., Urai, J.L., 2016. Dilatant normal faulting in jointed cohesive rocks: a physical model study. Solid Earth 7, 843–856. https://doi.org/10.5194/se-7-843-2016

Klinkmüller, M., Schreurs, G., Rosenau, M., Kemnitz, H. 2016. Properties of granular analogue model materials: A community wide survey. Tectonophysics 684, 23-38. http://dx.doi.org/10.1016/j.tecto.2016.01.017

Le Calvez, J.H., Vendeville, B.C., 2002. Experimental designs to model along-strike fault interaction, Journal of the Virtual Explorer 7, 1-17. https://doi.org/10.3809/jvirtex.2002.00043

Liao, J., and Gerya, T., 2015. From continental rifting to seafloor spreading: Insight from 3D thermo-mechanical modeling, Gondwana Res., 28, 1329-1343, http://dx.doi.org/10.1016/j.gr.2014.11.004

Maestrelli, D., Montanari, D., Corti, G., Del Ventisette, C., Moratti, G., Bonini, M., 2020 Exploring the interactions between rift propagation and inherited crustal fabrics through experimental modeling, Tectonics, 39, e2020TC006211. https://doi.org/10.1029/2020TC006211

Martín-Barajas, A., González-Escobar, M., Fletcher, J.M., Pacheco, M., Oskin, M., Dorsey, R., 2013. Thick deltaic sedimentation and detachment faulting delay the onset of continental rupture in the Northern Gulf of California: analysis of seismic reflection profiles. Tectonics 32, 1294–1311.
http://dx.doi.org/10.1002/tect.20063

McClay, K.R., White, M.J., 1995.Analogue modelling of orthogonal and oblique rifting, Mar. Petrol. Geol., 12, 137-151,
https://doi.org/10.1016/0264-8172(95)92835-K

Michon, L., Merle, O., 2000. Crustal structures of the Rhinegraben and the Massif Central grabens: An experimental approach, Tectonics, 19, 896– 904,
https://doi.org/10.1029/2000TC900015

Michon, L., and Merle, O., 2003. Mode of lithospheric extension: Conceptual models from analogue modeling, Tectonics, 22, 1028.
https://doi.org/10.1029/2002TC001435.

Molnar, N.E., A.R. Cruden, Betts, P.G., 2017. Interactions between propagat- ing rotational rifts and linear rheological heterogeneities: Insights from three- dimensional laboratory experiments, Tectonics, 36, 420–443.
https://doi.org/10.1002/2016TC004447

Molnar, N.E., A.R. Cruden, Betts, P.G., 2018. Unzipping continents and the birth of microcontinents, Geology 46, 451-454.
https://doi.org/10.1130/G40021.1

Molnar, N.E., A.R. Cruden, Betts, P.G., 2019. Interactions between propagating rifts and linear weaknesses in the lower crust, Geosphere 15.
https://doi.org/10.1130/GES02119.1

Molnar, N.E., A.R. Cruden, Betts, P.G., 2020. The role of inherited crustal and lithospheric architecture during the evolution of the Red Sea: Insights from three dimensional analogue experiments, Earth Planet. Sc. Lett., 544, 116377.
https://doi.org/10.1016/j.epsl.2020.116377

Morley, C.K., Nelson, R.A., Patton, T.L., Munn, S.G., 1990. Transfer Zones in the East African Rift System and Their Relevance to Hydrocarbon Exploration in Rifts, AAPG Bull., 74, 1234-1253.
https://doi.org/10.1306/0C9B2475-1710-11D7-8645000102C1865D, 1990.

Morley, C.K., 2010. Stress re-orientation along zones of weak fabrics in rifts: An explanation for pure extension in ‘oblique’ rift segments? Earth Planet. Sc. Lett. 297, 667-673.
https://doi.org/10.1016/j.epsl.2010.07.022

Mulugeta, G., 1988. Squeeze box in a centrifuge, Tectonophysics 148, 323-335.
https://doi.org/10.1016/0040-1951(88)90139-4

Naylor, M.A., Laroque, J.M., Gauthier, B.D.M., 1994. Understanding extensional tectonics: insights from sandbox models, International Symposium on Geodynamic Evolution of Sedimentary Basins, Moscow (Russian Federation). Technip, 92 (France), https://www.osti.gov/etdeweb/biblio/399440

Nelson, R.A., Patton, T.L., Morley, C.K., 1992. Rift-Segment Interaction and Its Relation to Hydrocarbon Exploration in Continental Rift Systems (1), AAPG Bull., 76, 1153-1169. https://doi.org/10.1306/BDFF898E-1718-11D7-8645000102C1865D

Nestola, Y., Storti, F., Cavozzi, C., 2015. Strain rate-dependent lithosphere rifting and necking architectures in analog experiments, J. Geophys. Res. Solid Earth. 120, 584–594. https://doi.org/10.1002/2014JB011623

Oliveira, M.E., Gomes, A.S., Rosas, F.M., Duarte, J.C., França, G.S., Almeida, J.C., Fuchk, R.A., (*in review*). Double-rift nucleation above inherited crustal weaknesses: insights from 2D numerical models. Tectonophysics

Panien, M., Schreurs, G., Pfiffner, A., 2006. Mechanical behaviour of granular materials used in analogue modelling: insights from grain characterisation, ring-shear tests and analogue experiments, J. Struct. Geol., 28, 1710-1724. https://doi.org/10.1016/j.jsg.2006.05.004

Phillips, T.B., Fazlikhani, H., Gawthorpe, R.L., Fossen, H., Jackson, C.A. ‐ L., Bell, R.E., Faleide, J.I., Rotevatn, A., 2019. The influence of structural inheritance and multiphase extension on rift development, the northern North Sea. Tectonics, 38, 4099–4126. https://doi.org/10.1029/2019TC005756

Ramberg, H. 1981. Gravity, Deformation and the Earth's Crust. Academic Press, London, United Kingdom.

Reeve, M.T., Bell, R.E., Duffy, O.B., Jackson, C.A.-L., Sansom, E., 2015. The growth of non-colinear normal fault systems; What can we learn from 3D seismic reflection data? Journal of Structural Geology 70, 141-155. http://dx.doi.org/10.1016/j.jsg.2014.11.007

Reiter, K. 2021. Stress rotation – impact and interaction of rock stiffness and faults. Solid Earth 12, 1287-1307. https://doi.org/10.5194/se-12-1287-2021

Rudolf, M., Boutelier, D., Rosenaus, M., Schreurs, G., Oncken, O., 2016. Rheological benchmark of silicone oils used for analog modeling of short- and long-term lithospheric deformation, Tectonophyiscs 684, 12-22. http://dx.doi.org/10.1016/j.tecto.2015.11.028

Ruh, J.B., 2019. Effects of fault-weakening processes and oblique intracontinental rifting and subsequent inversion. Am. J. Geosc. 319, 315-338. https://doi.org/10.2475/04.2019.03

Samsu, A., Cruden, A.R., Hall, M., Micklethwaite, S., Denyszyn, S.W., 2019. The influence of basement faults on local extension directions: Insights from potential field geophysics and field observations, Basin Res. 31, 782-807. https://doi.org/10.1111/bre.12344

Saria, E., Calais, E., Stamps, D.S., Delvaux, D., Hartnady, C.J.H., 2014. Present-day kinematics of the East African Rift, J. Geophys. Res-Sol. Ea., 119, 3584-3600. https://doi.org/10.1002/2013JB010901

Schlagenhauf, A., Manighetti, I., Malavieille, J., Dominguez, S. 2008. Incremental growth of normal faults: Insights from a laser-equipped analog experiment. Ea. Planet. Sci. Lett. 273, 299-311. https://doi.org/10.1016/j.epsl.2008.06.042

Tron, V., Brun, J.-P., 1991. Experiments on oblique rifting in brittle-ductile systems, 188, 71-84. https://doi.org/10.1016/0040-1951(91)90315-J

Twiss, R.J., Moore, E.M. 1992. Structural Geology. W.H. Freeman and Company, New York, United States of America.

Van Wijk, J.W., 2005. Role of weak zone orientation in continental lithosphere extension. Geophys. Res. Lett. 31, L02303. https://doi.org/10.1029/2004GL022192

Virgo, S., Abe, S., Urai, J.L., 2014. The evolution of crack seal vein and fracture networks in an evolving stress field: Insights from Discrete Element Models of fracture sealing. J. Geophys. Res-Sol. Ea. 119, 8708-8727. https://doi.org/10.1002/2014JB011520

Weijermars, R., Schmeling, H., 1986. Scaling of Newtonian and non-Newtonian fluid dynamics without inertia for quantitative modelling of rock flow due to gravity (including the concept of rheological similarity), Phys. Earth. Planet. In., 43, 316-330, https://doi.org/10.1016/0031-9201(86)90021-X

Wenker, S., Beaumont, C., 2018. Can metasomatic weakening result in the rifting of cratons?, Tectonophysics 746, 3-21. http://dx.doi.org/10.1016/j.tecto.2017.06.013

Wang, L., Maestrelli, D., Corti, G., Zou, Y., Shen, C., 2021. Normal fault reactivation during multiphase extension: Analogue models and application to the Turkana Depression, East Africa, Tectonophysics, 811. https://doi.org/10.1016/j.tcto.2021.228870

Wilson, J. T., 1966. Did the Atlantic Close and then Re-Open?, Nature 211, 676-681, https://doi.org/10.1038/211676a0

Withjack, M.O., Henza, A.A., Schlische, R.W., 2017. Three-dimensional fault geometries and interactions within experimental models of multiphase extension. AAPG Bull., 101, 1767-1789.

https://doi.org/10.1306/02071716090

Zwaan, F., Schreurs, G.: How oblique extension and structural inheritance influence rift segment interaction: Insights from 4D analog models, Interpretation 5, SD119-138, http://dx.doi.org/10.1190/INT-2016-0063.1, 2017.

Zwaan, F, Schreurs, G. 2021 Analogue modelling of continental rifting: an overview. In: Peron-Pinvidic (ed.): Rifted Margins, ISTE-WILEY. 2021. https://www.researchgate.net/publication/349536310_Analogue_modelling_of_continental_rifting_an_overview

Zwaan, F., Schreurs, G., Naliboff, J., Buiter, S.J.H., 2016. Insights into the effects of oblique extension on continental rift interaction from 3D analogue and numerical models, Tectonophysics 693, 239-260. http://dx.doi.org/10.1016/j.tecto.2016.02.036

Zwaan, F., Schreurs, G., Adam, J., 2018a. Effects of sedimentation on rift segment evolution and rift interaction in orthogonal and oblique extensional settings: Insights from analogue models analysed with 4D X-ray computed tomography and digital volume correlation techniques, Global Planet. Change, 171, 110-133. https://doi.org/10.1016/j.gloplacha.2017.11.002

Zwaan, F., Schreurs, G., Gentzmann, R., Warsitzka, M., Rosenau, M., 2018b. Ring-shear test data of quartz sand from the Tectonic Modelling Lab of the University of Bern (CH). GFZ Data Services. https://doi.org/10.5880/fidgeo.2018.028

Zwaan, F., Schreurs, G., Ritter, M., Santimano, T., Rosenau, M., 2018c. Rheology of PDMS-corundum sand mixtures from the Tectonic Modelling Lab of the University of Bern (CH), GFZ Data Services. https://doi.org/10.5880/fidgeo.2018.023

Zwaan, F., Schreurs, G., Buiter, S.J.H., 2019. A systematic comparison of experimental set-ups for modelling extensional tectonics, Solid Earth 10, 1063-1097, https://doi.org/10.5194/se-10-1063-2019

Zwaan, F., Corti, G., Keir, D., Sani, F., 2020a. A review of tectonic models for the rifted margin of Afar: implications for continental break-up and passive margin formation. J. Afr. Earth Sci. 164, 103649. https://doi.org/10.1016/j.jafrearsci.2019.103649

Zwaan, F., Corti, G., Keir, D., Sani, F., 2020b. Analogue modelling of marginal flexure in Afar, East Africa: Implications for passive margin formation. Tectonophysics 796, 228595. https://doi.org/10.1016/j.tecto.2020.228595

Zwaan, F., Corti, G., Sani, F., Keir, D., Muluneh, A., Papini, M., 2020c. Structural analysis of the Western Afar Margin, East Africa: evidence for multiphase rotational rifting. Tectonics 39, e2019TC006043. https://doi.org/10.1029/2019TC006043.

Zwaan, F., Schreurs, G., and Rosenau, M., 2020d. Rift propagation in rotational versus orthogonal extension: Insights from 4D analogue models, J. Struct. Geol. 135, 103946, https://doi.org/10.1016/j.jsg.2019.103946

Zwaan, F., Chenin, P., Erratt, D., Manatschal, G., Schreurs, G., 2021a. Complex rift patterns, a result of interacting crustal and mantle weaknesses, or multiphase rifting? Insights from analogue models. Solid Earth 12, 1473-1495. https://doi.org/10.5194/se-12-1473-2021

Zwaan, F., Chenin, P., Erratt, D., Manatschal, G., Schreurs, G., 2021b. PIV and topographic analysis data from analogue experiments involving 3D structural inheritance and multiphase rifting. GFZ Data Services. Temporary link: https://www.dropbox.com/sh/ousqc4hqyq5nd5p/AACB9hpYnx-8ww0EdpjUsI6ma?dl=0